Received: 25 October 2021 | Revised: 27 February 2022 | Accepted: 7 March 2022

DOI: 10.1002/suco.202100754

ARTICLE

fib CEB-FIP WILEY

Slender precast voided slabs under walking-induced vibration

Bruno Dal Lago[1] | **Luca Martinelli**[2] | **Francesco Foti**[2]

[1]Department of Theoretical and Applied Sciences, Università degli Studi dell'Insubria, Varese, Italy

[2]Department of Civil and Environmental Engineering, Politecnico di Milano, Milan, Italy

Correspondence
Bruno Dal Lago, Department of Theoretical and Applied Sciences, Università Degli Studi dell'Insubria, via Dunant, 3, 21100 Varese, Italy.
Email: bruno.dallago@uninsubria.it

Abstract

Disturbance/discomfort caused by vibrations, induced by pedestrian walking on slabs in residential/office buildings, is a typical design issue for lightweight slender slabs, including prestressed concrete ones. Precast slabs are typically made with pretensioned members which allow for only partial collaboration in the transverse slab direction, which becomes even less effective when they are dry-assembled without cast-in-situ topping since it relies on the arrangement of mutual mechanical connections only. This study investigates through tests and numerical analyses the response of slender precast long-span slabs made with voided members, dry-assembled with mechanical connections, when subjected to vibrations generated by human activities. A parametric set of dynamic modal and time-history analyses encompassing floor member geometry, connection arrangement, mass, and damping, is carried out. The numerical models are validated against results from an experimental test program carried out on two decks of a prototype precast building. The tests and the numerical models allowed to characterize the fundamental dynamic properties of the slab and its vibrational performance, identifying the most efficient technological solutions among those investigated to mitigate human-induced vibrations

KEYWORDS

vibrations, discomfort, precast structures, prestressed slabs, smartphone-assisted testing, numerical simulation, design against vibrations

1 | INTRODUCTION

The evolution of the production technologies in the field of precast concrete constructions brought to the development of particularly slender and structurally optimized prestressed floor elements. Within the European scenario, the relentless quest toward daring precast decks, started in the 1950s, recently brought to the definition of standard production lines with span up to 42 m for roof elements.[1] Due to their peculiar slenderness, the critical design issue for these prestressed elements, which are also used as secondary beams in industrial single-storey frames, is frequently deflection control at the Serviceability Limit State (SLS) rather than resistance at the

Discussion on this paper must be submitted within two months of the print publication. The discussion will then be published in print, along with the authors' closure, if any, approximately nine months after the print publication.

Ultimate Limit State (ULS).[2] Based on the achievements in the field of industrial constructions, pretensioned long-span decks have been successfully introduced since the 1970s in the field of commercial structures (parking facilities, malls, etc.), typically in buildings with less than five stories, characterized by large span and heavy live loads. Contemporarily, residential precast buildings employed shorter spans, typically not longer than 10 m, using partially precast elements having relevant mass. Recently, the employment of slender lightweight prestressed slabs is increasing worldwide in the construction field of multistorey buildings of residential/office use. Thanks to the incorporation of the Mechanical, Electrical and Plumbing (MEP) equipment distribution inside the slab, floor elements spanning up to 12 m have been proposed with total slab depth (including technological layers and finishes) of 40–45 cm, which is comparable to the thickness of cast-in-situ slabs having much shorter spans. Among the serviceability checks required in design, vibration may become the critical one due to the peculiar slenderness of the slabs combined with low volume of concrete employed and, therefore, mass.

Vibration in service has been rarely considered a design issue for reinforced concrete slabs in buildings, being it typically more critical in steel or timber flooring technologies (indeed, while cited among the SLSs in the European code that describes the basis for the design and verification of structures—Eurocode 0[3]—it is not treated in detail inside the European code that describes the design and detailing of reinforced concrete structures—Eurocode 2[4]). As such, information in literature about this subject are relatively scarce. After the pioneering framing of the problem,[5–7] the topic of vibrations in service of concrete structures has been assessed in literature mainly referring to pedestrian bridges[8–11] and cast-in-situ concrete floors,[12–17] eventually posttensioned, although few papers were recently published about the issue of human-induced vibration on precast pretensioned concrete hollow core members.[18,19] It is also worth recalling that those elements are characterized by similar slenderness with respect to the floor element analyzed in this paper, but higher mass due to the higher concrete volume employed.

While the issue of structural vibrations in service is only marginally treated in the general structural codes, the main issues related to the definition of the human walking action[20–23] and human perception of vibrations[24–26] have been included into the current specific standards. Two approaches for the check of human-induced vibrations in service can be identified: (1) a deterministic approach, like the one adopted by the International Standard for the evaluation of structures against vibrations (ISO 10137:2007),[27] from which many national standards including the Italian (UNI 9614:1990)[28] were derived, and (2) a probabilistic approach, like that of the HIVOSS guidelines.[29,30] The first one refers to limit values of deck acceleration expressed in terms of root mean square (RMS):

$$\mathrm{RMS} = \sqrt{\frac{1}{T}\int_0^T a^2(t)dt}, \tag{1}$$

where a is the acceleration, T is the time window over which the RMS value is computed, and t is the time.

The probabilistic approach of the HIVOSS guidelines,[29,30] on the other hand, refines this concept by making reference to performance classes of the deck, based on RMS values computed over T equal to the duration of one step, corresponding to a prescribed probability (90%) not to be exceeded (one step-root mean square [OS-RMS_{90}]) considering 700 input signals of human walking characterized by different step frequency and pedestrian mass.

This paper analyses the vibrational response of peculiar dry-assembled lightweight slender precast slabs through a parametric set of dynamic modal and time-history analyses investigating the effect of transverse restraint conditions (connection arrangement), floor member depth, mass, and damping in mitigating the perception of vibrations. Numerical models set for the above purpose have been validated against the results of a test program encompassing heel-drop impact, walk-in-place, and walking tests on two decks of a building prototype adopting the new prestressed slab technology under investigation.

2 | PRESTRESSED SLABS UNDER INVESTIGATION

Two physically constructed prestressed decks are included in this study. The decks are part of a prototype building of a novel precast construction system for housing.[31,32] They are made by 2.4 m wide and 0.35 m deep precast elements having box cross-section with lower flange, as described in Figure 1 together with the position of the main prestressing tendons. Pictures from the 3D BIM model of the prototype are shown in Figure 2. The elements of the ground floor deck, supported on an inverted-T shaped foundation beam, are 11.0 m long and are provided with steel plate inserts for mutual connection in six points along the lower flange as well as at midspan in the ribs. The elements of the roof deck are supported on two bearing wall elements and are 11.2 m long. They are provided with steel plate inserts for mutual connection in six points along the lower flange only. Mutual floor connections made by steel bars welded to metallic angle inserts of adjacent flanges[33,34] are introduced

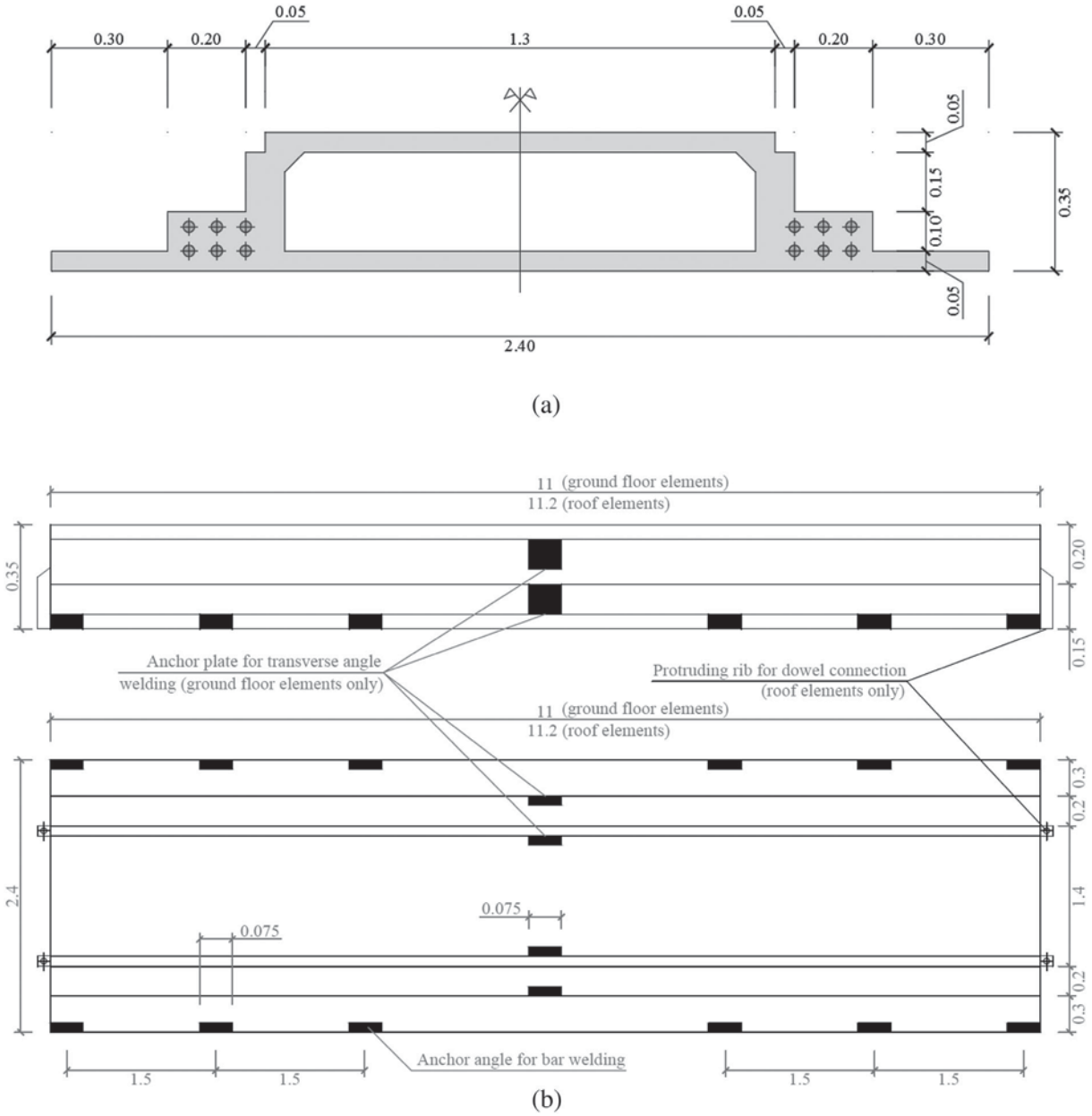

FIGURE 1 Prestressed (pretensioned) floor element: (a) cross-section with position of main prestressing tendons; (b) lateral and top views with positions of transverse floor-to-floor connections

for improvement of the in-plane diaphragm action under horizontal loads induced by earthquake, wind or exceptional loads.[35–37]

Additional mutual floor connections made by X-shaped steel angles L100 × 100 × 8 welded to the plate inserts in the ribs exclusively at midspan provide a transverse load repartition beam aimed at improving the interaction of the floor elements when the deck is subjected to concentrated loads.

Four floor elements per deck are placed adjacently and 5-cm deep secondary concrete solid plates are interposed in simple support over the rib recesses of the floor elements and, at the edges, of the cladding panels, to create a flat surface. Figure 3 shows pictures of the constructed prototype including the mutual floor welded bar connections (Figure 3c) in the flanges and the transverse X-shaped steel angles (Figure 3d). These are present in the ground deck only, and it is specified that they are not employed for the connection of the edge floor elements with the peripheral cladding panels.

As a difference between the drawings and the real prototype, at the ground floor the secondary slab plates were installed only on half of the span; at the roof the secondary slab plates were not installed at all.

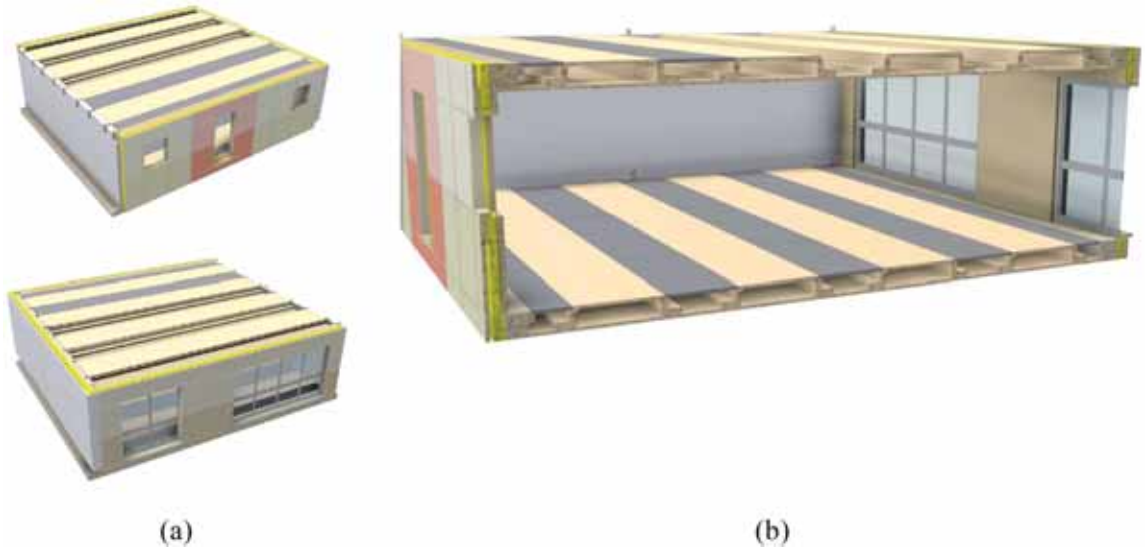

FIGURE 2 3D BIM drawing of the prototype building: (a) assembled views; (b) vertical section cutting slab and cladding panel elements

Concrete class C45/55, high-strength steel (nominal tensile strength of 1860 MPa) for prestressing tendons, steel grade B450C for rebars, and steel grade S235 for angles, were adopted.

Note that similar decks have been previously constructed and tested under earthquake action in the ELSA laboratory of the Joint Research Centre (JRC) within the Safecast research project,[38–41] although with objectives and floor span lengths different than in the present paper.

3 | EXPERIMENTAL PROGRAM AND EQUIPMENT

An experimental program encompassing a total of 26 tests has been carried out on both ground and roof decks, with longitudinal (LONG) or transverse (TRANS) disposition of the instrumentation with reference to the axis of the floor element (Figure 4), with different load types including heel-drop, walk-in-place, and promenade walking with different walking paths (Figure 4), and with two different pedestrians. A simplified experimental evaluation of the floor vibration was carried out with the aim to check the numerical modeling strategies presented in the following, by means of the above-described load types, following suggestions routinely found in the literature.[42] The complete list is given in Table 1.

Pictures during testing for both instrument dispositions herein adopted are collected in Figure 5.

The mass of Pedestrians A and B is approximately 92 and 90 kg, respectively. Both were wearing casual shoes (desert boots) with rubber soles. Pedestrian A has flat feet. As derived from the instrumentation installed over the pedestrians, the mean step length of Pedestrians A and B is approximately 0.84 and 0.91 m, respectively, while the mean step frequency (period) of pedestrians A and B is approximately 1.63 (0.61 s) and 2.07 Hz (0.48 s), respectively. This will be described below.

Both standard and nonstandard instrumentation has been employed in the experimental program.[43] Four professional mono-axial piezoelectric accelerometers type Wilcoxon Research Model 731A (Figure 6a) with acquisition frequency of 200 Hz installed over solid steel stabilizing blocks were connected to a signal acquisition unit type National Instruments NI-9234. The signal acquisition unit was then linked to a computer logger (Figure 6b) where the signal was recorded with a Labview software.[44] The logger station was placed outside of the prototype building in the position indicated in Figure 4 so to avoid any possible interaction with the decks. Accelerations were also recorded with a commercial smartphone, model Huawei Y5 DRA L21 issued in 2018 provided with a tri-axial MEMS accelerometer with mean acquisition frequency of 200 Hz. The smartphone was alternatively put in adjacency to a professional accelerometer (Figure 6a) with the aim to check its suitability in signal recording, as well as tied firmly with a belt right above the waist (close to the center of gravity) of the pedestrian with the aim to record the input signal. This position tends to minimize the disturbance induced by horizontal translation and rotations occurring during walking. The free application "Physics Toolbox"[45] was installed in the device and was used to record the signal. As a matter of fact, the current popular smartphones are provided with sophisticated high-precision accelerometers installed for matters other than scientific, and their possible

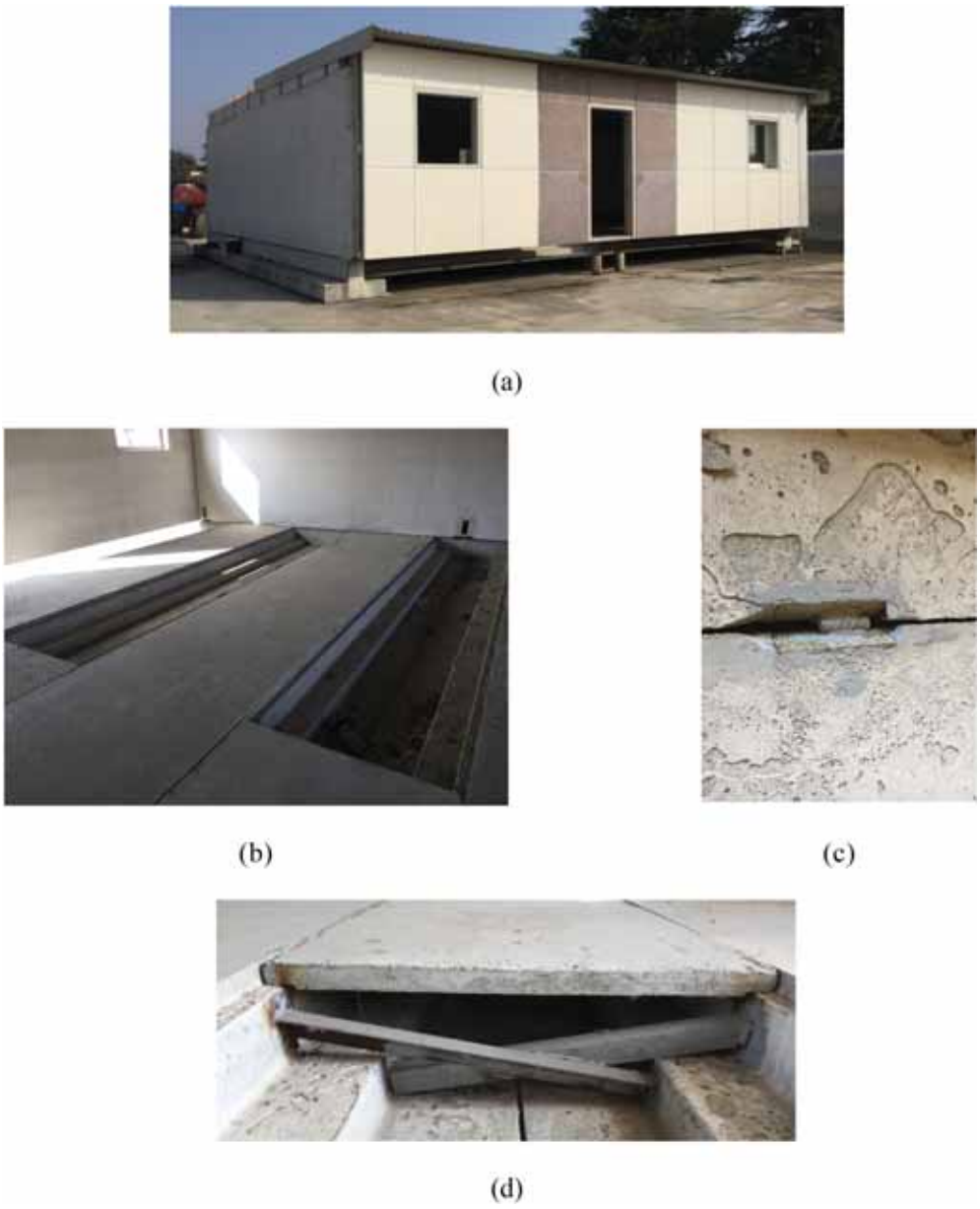

FIGURE 3 Pictures of the prototype building: (a) view from south-east side; (b) inner view of ground floor deck; (c) particular view of a floor-to-floor welded connection; (d) particular view of a metallic X-shaped transverse brace

implementation in structural monitoring could become an important aid during field testing, as also pointed out in the works decribed.[43,46–49]

4 | MAIN EXPERIMENTAL RESULTS

A fast Fourier Transform analysis has been carried out on all recorded signals, allowing the identification of the acceleration spectra characteristics of each deck, reported in Figure 7. Unless specified, in the following signals recorded by Wilcoxon accelerometers located at stations from A1 to A4 (see Figure 4) will be used. The results of different tests on the same deck provided very similar spectra, as expected. Table 2 reports the identified frequencies of the first four modes of the decks, corresponding to the peaks of the acceleration spectrum (Figure 7). The frequencies of the two decks have differences attributable to both a slightly different length of the floor elements (11.0 m the ground deck; 11.2 m the roof deck), a different mass (the roof deck lacks the secondary concrete slab plates), and a different transverse restraint condition (since the ground deck has a central repartition beam, while the roof deck is without it).

It results that the decks under investigation have fundamental natural frequency in between 7 and 10 Hz, range considered in the literature as the threshold between low-frequency and high-frequency decks, although recently there are proposals to move this threshold[50] to higher frequencies values. In low-frequency decks, the transient response to human walking tends to a stationary vibration

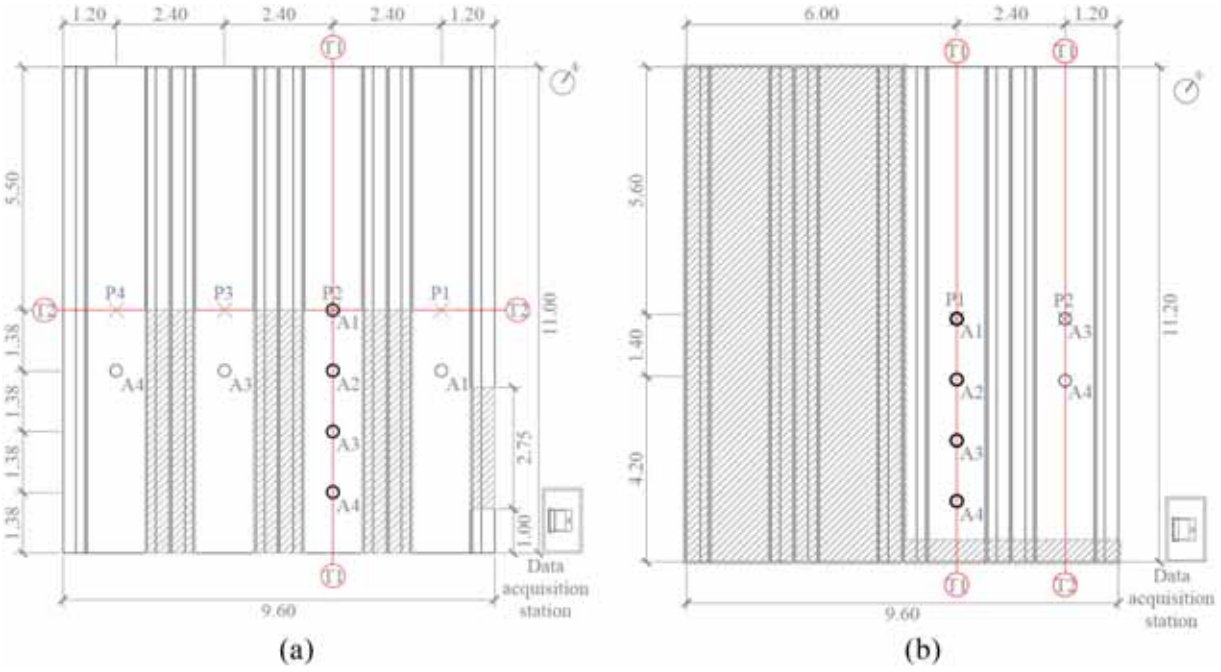

FIGURE 4 Position of instruments and load paths: (a) ground floor deck; (b) roof deck. Note that transverse and longitudinal accelerometers dispositions are alternative

(Figure 8a); in high-frequency decks, the response to human walking is always in the transient phase, with the vibration almost extinguishing between steps (Figure 8b). Slabs with a fundamental frequency close to the threshold, like the ones under consideration in this paper, are typically the most complex to be addressed due to the coexistence of the two behaviors. The modal shapes associated to the different frequencies will be discussed in detail in the next chapter in comparison with those resulting from the numerical model. The modal Equivalent Viscous Dampings (EVD) has been calculated according to the classical method of logarithmic decrement.[51] The values, reported in Table 2, range in between 0.9% and 1.1% of the critical for the first 3 modes, lowering to 0.7%–0.8% for the 4th. Such low values are consistent with the absence of any finishing, partition, and furniture on the tested decks, being them part of a structural building prototype.

Typical acceleration time histories resulting from heel-drop tests are shown in Figure 9 with reference to two different instrument dispositions. For each accelerometer, negative peak, positive peak, and RMS accelerations over time windows of 10 s for Pedestrian A, and 7 s for Pedestrian B, corresponding to the time the pedestrians employed to walk along the whole slab length, are collected in Table 3 for both decks and for both instrument dispositions. In the case of heel-drop tests the higher RMS value is always associated with the accelerometer closer to the position of the pedestrian during the heel-drop.

Typical acceleration time histories resulting from walking tests are shown in Figure 10 with reference to two different pedestrians. For each accelerometer, negative peak, positive peak, and RMS accelerations are collected in Table 4 for both decks and both pedestrians. Despite the formal similitude of Tests #3 and #4, which differ only from the pedestrian, the results highlight that Pedestrian B induces more severe vibrations than Pedestrian A, with an about 2.5 times higher RMS value. It is also worth observing that the maximum RMS acceleration value among the three walking tests reported in Table 4 is that of the roof deck with Pedestrian A. This may depend upon the different responses of the decks but also on a different walking style of the same pedestrian through the tests. A deck vibrational response intermediate between low- and high-frequency as previously discussed is confirmed by observing the acceleration histories of Figure 10, with a trend intermediate between the two depicted in Figure 8.

The signal recorded by smartphones installed on the back of the pedestrians, considered reliable after validation as discussed in detail in Martinelli et al.,[43] has been considered for a better definition of the load in the numerical analyses. The smartphone signals, shown in Figure 11, confirm the different walking style of pedestrians A and B both in terms of acceleration time history and of frequency content. It is to be noted that the walking of Pedestrian B is characterized by frequencies around 2 Hz and multiples of this, thus more resembling

TABLE 1 List of the dynamic tests performed

Test ID	Deck	Instrument disposition	Load type	Load path	Pedestrian	Notes
#1	Ground	Long	Heel-drop	P2	A	Smartphone next to A2
#2	Ground	Long	Walk in place	P2	A	Smartphone next to A2
#3	Ground	Long	Walking	T1	A	Smartphone on pedestrian
#4	Ground	Long	Walking	T1	B	Smartphone on pedestrian
#5	Ground	Long	Walking	T1	A	Pedestrian B in A2
#6	Ground	Long	Heel-drop	P4	A	Smartphone next to A2
#7	Ground	Long	Heel-drop	P3	A	Smartphone next to A2
#8	Ground	Long	Heel-drop	P1	A	Smartphone next to A2
#9	Ground	Long	Walking	T2	A	Smartphone next to A2
#10	Ground	trans	Heel-drop	P2	A	Smartphone next to A2
#11	Ground	trans	Walk in place	P2	A	Smartphone next to A2
#12	Ground	trans	Walking	T1	A	Smartphone on pedestrian
#13	Ground	trans	Walking	T1	B	Smartphone on pedestrian
#14	Ground	trans	Walking	T1	A	Pedestrian B in A2
#15	Ground	trans	Heel-drop	P4	A	-
#16	Ground	trans	Heel-drop	P3	A	-
#17	Ground	trans	Heel-drop	P1	A	-
#18	Ground	trans	Walking	T2	A	-
#19	Ground	trans	Walking	T1	A + B	-
#20	Roof	Long	Heel-drop	P1	A	-
#21	Roof	Long	Walking	T1	A	-
#22	Roof	Long	Heel-drop	P2	A	-
#23	Roof	Trans	Heel-drop	P1	A	-
#24	Roof	Trans	Walking	T1	A	-
#25	Roof	Trans	Heel-drop	P2	A	-
#26	Roof	Trans	Walking	T2	A	-

FIGURE 5 Pictures of instrument disposition and loading: (a) walking test with longitudinal instrument disposition; (b) heel-drop impact or walk in place test with transverse instrument disposition

FIGURE 6 Experimental equipment: (a) professional accelerometers and smartphone; (b) logger station with cable collector box placed outside the prototype building

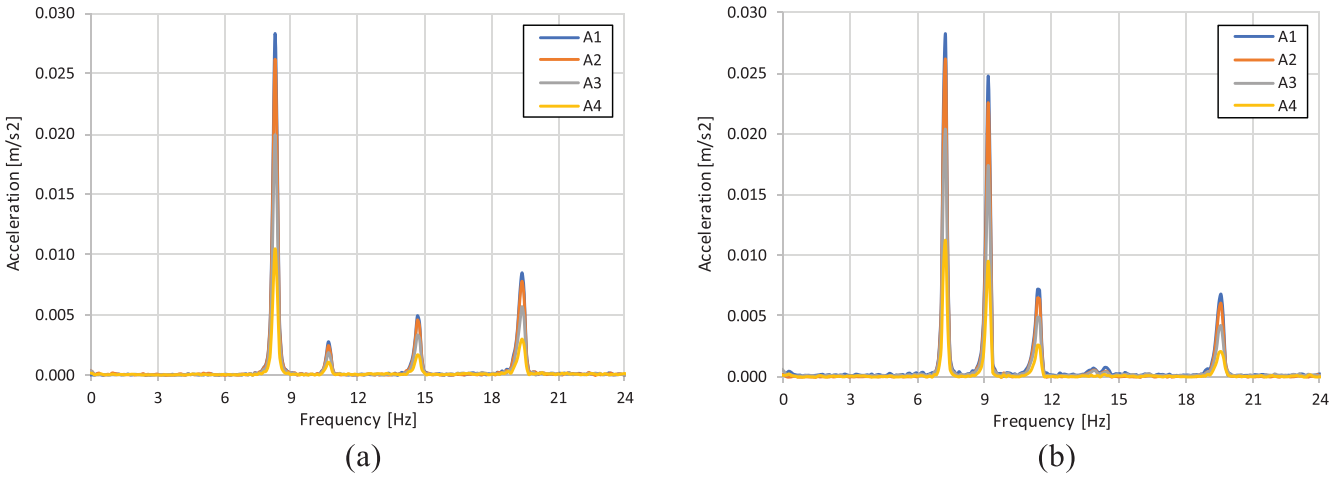

FIGURE 7 Frequency spectrum content of: (a) ground floor deck (Test #1); (b) roof deck (Test #20)

TABLE 2 Natural vibration frequencies and damping from Tests #1 and #20

	Frequency (Hz)		Damping (%)	
Floor	Ground	Roof	Ground	Roof
Mode 1	8.296	7.296	1.032	1.114
Mode 2	10.695	9.195	1.040	0.986
Mode 3	14.693	11.494	0.908	0.910
Mode 4	19.390	19.590	0.801	0.669

to the classical frequency content considered in the scientific literature for steps[8] and in the standards.

5 | NUMERICAL SIMULATION: DYNAMIC PROPERTIES

Numerical models have been built with Midas Gen software[52] with two aims: (a) identifying the proper modeling technique by comparison with the experimental data, and (b) performing a parametric analysis to target the physical quantities which mostly influence the vibrational problem of the deck technology under investigation.

Plate elements with side length not larger than 0.2 m and thickness of 5, 10, and 15 cm have been used to model the floor elements regarding upper and lower flanges, ribs, and prestressing bulbs in lower flange, respectively. Proper offsets have been applied to accurately simulate the real position of thicker flange elements. Beam elements have been used to model the transverse X-shaped load repartition elements. All nodes are fixed to the adjacent ones. Along the edges of adjacent floor elements spaced by 10 mm, the two nodes corresponding to the center of gravity along floor axis of the mutual floor-to-floor welded bar connections have been linked with a rigid element simulating a cylindrical hinge linking all translations and rotations along X and Z axes. The rotation along Y-axis, torsional with respect to the floor element, has not been restrained. The mass has been modeled as spread through the attribution of the material density to the elements. For the ground deck only, the presence of the upper solid slab plates on only half of the span has been taken into account with a

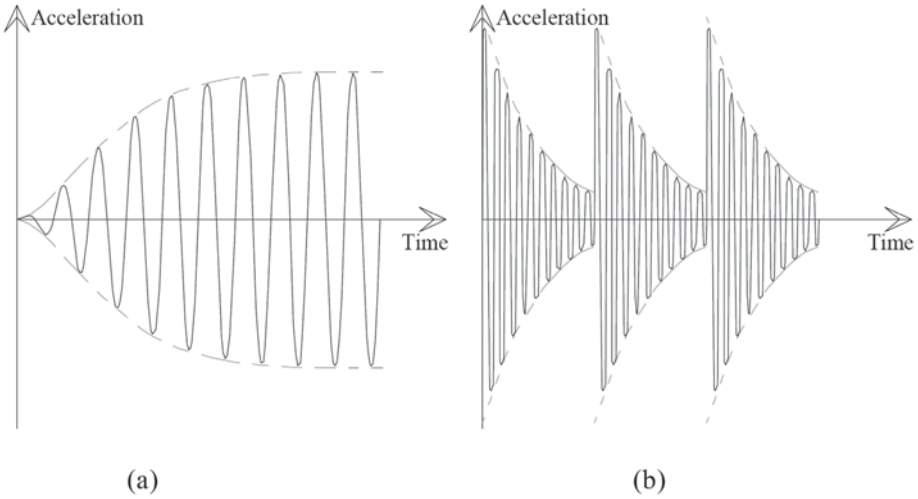

FIGURE 8 Vibration response types for decks: (a) low-frequency decks with transient response tending to a stationary level; (b) high-frequency decks with full impulse-like response

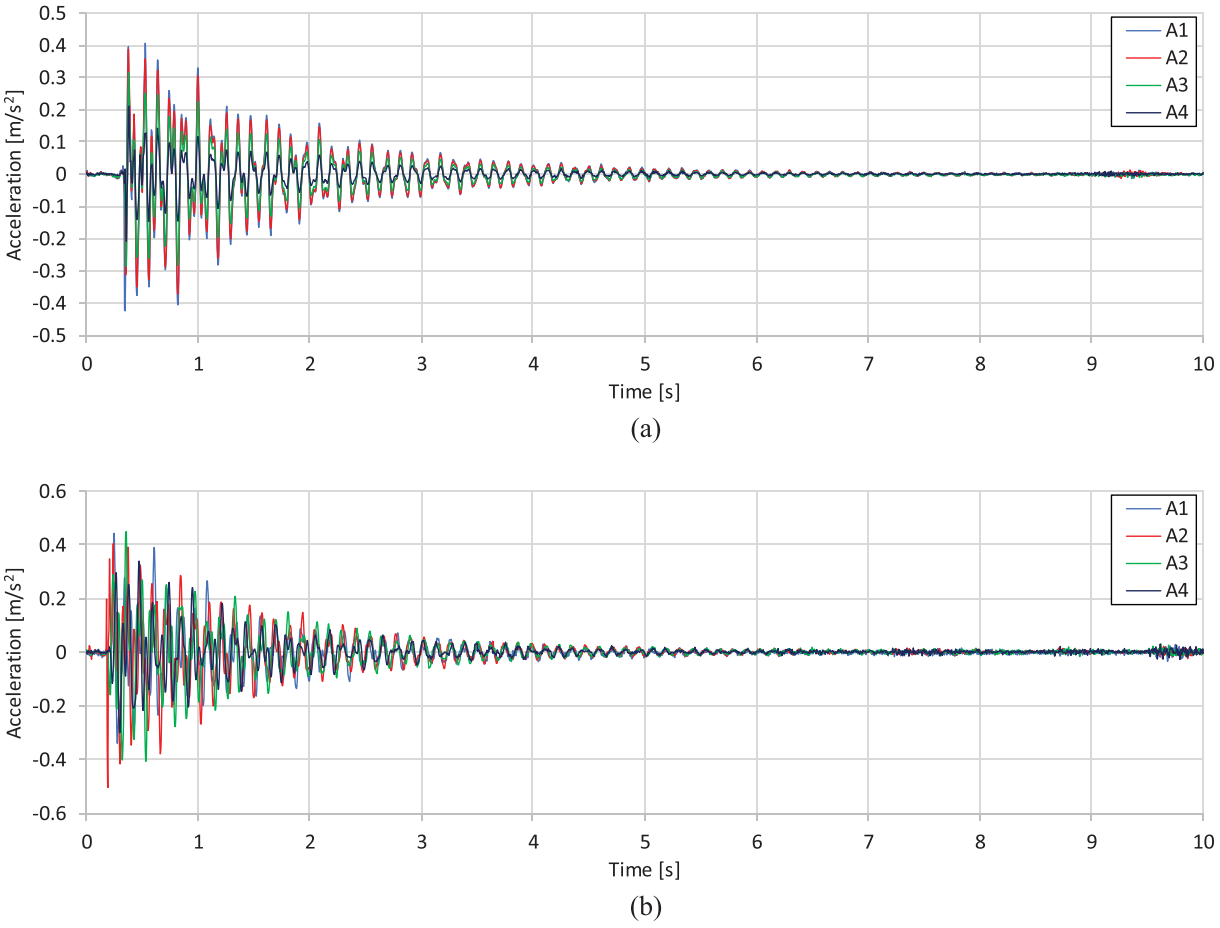

FIGURE 9 Experimental results of heel-drop impact tests: (a) Test #1; (b) Test #10

uniform additional linear mass distribution on the ribs in the proper region.

Linear elastic behavior has been considered: a mean Young modulus of 37.27 GPa and a Poisson coefficient of 0.2 as per Eurocode 2[4] for class C50/60 concrete (a higher class with respect to the one prescribed has been considered following standard compressive tests on concrete cubes carried out by the producer); a mean Young modulus of 210 GPa and a Poisson coefficient of 0.3 as per Eurocode 3[53] for steel (used to model the transverse repartition beam elements).

Two different external boundary conditions have been considered at the floor elements ends: (a) hinged, and (b) clamped. The results from the modal analysis

TABLE 3 Results of heel-drop impact tests

Test ID	Accelerometer	Peak—negative (m/s^2)	Peak—positive (m/s^2)	RMS (m/s^2)
#1	1	−0.415	0.397	**0.0645**
	2	−0.363	0.380	0.0588
	3	−0.278	0.308	0.0446
	4	−0.204	0.205	0.0241
#10	1	−0.399	0.346	**0.0567**
	2	−0.350	0.391	0.0532
	3	−0.391	0.458	0.0551
	4	−0.349	0.389	0.0484
#20	1	−0.666	0.546	**0.0814**
	2	−0.787	0.629	0.0759
	3	−0.602	0.570	0.0580
	4	−0.560	0.330	0.0336
#23	1	−0.653	0.593	**0.0749**
	2	−0.567	0.668	0.0688
	3	−0.417	0.565	0.0661
	4	−0.380	0.462	0.0594

Note: The higher values of RMS acceleration are in bold.

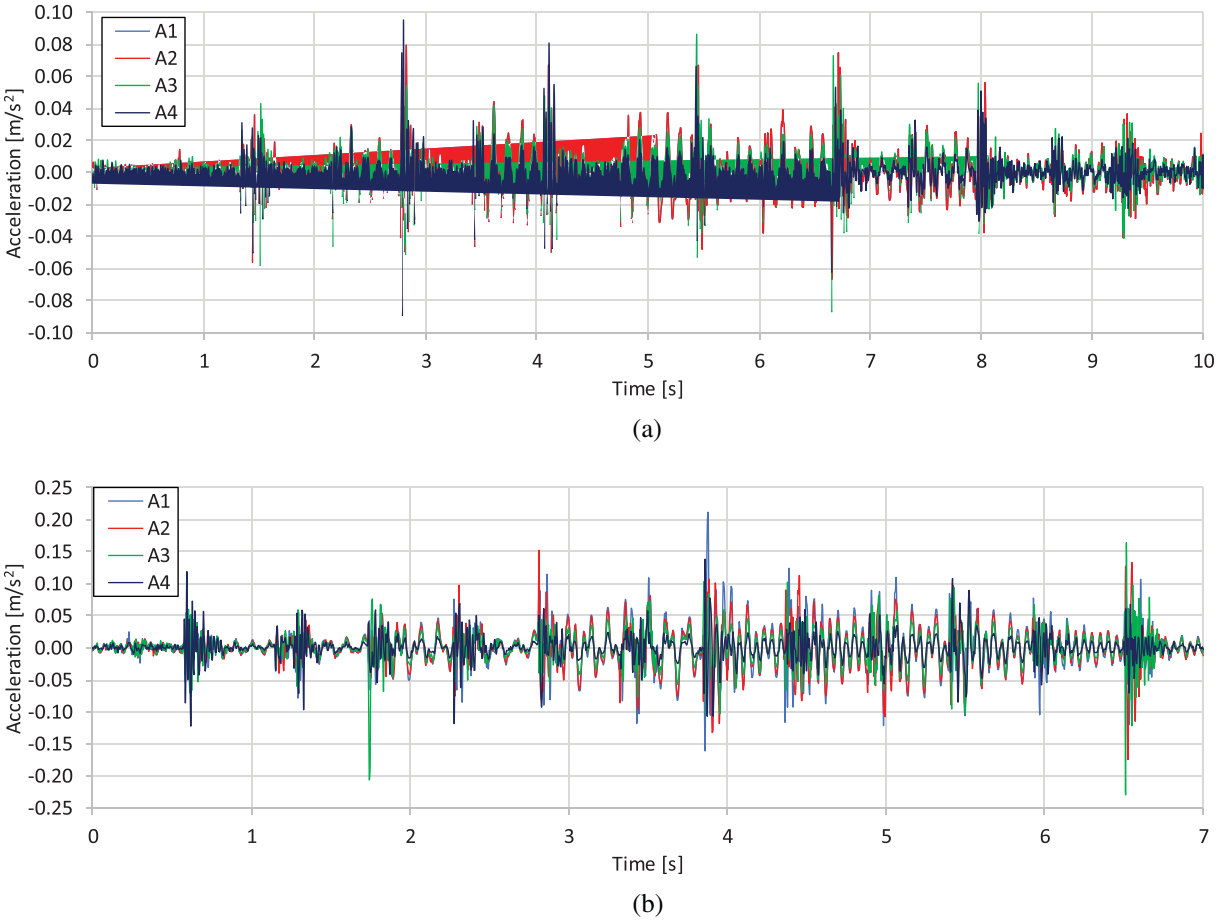

FIGURE 10 Experimental results of walking tests: (a) Test #3; (b) Test #4

TABLE 4 Results of walking tests

Test ID	Accelerometer	Peak—negative (m/s^2)	Peak—positive (m/s^2)	RMS (m/s^2)
#3	1	−0.060	0.094	**0.0136**
	2	−0.067	0.079	0.0132
	3	−0.087	0.082	0.0117
	4	−0.089	0.092	0.0096
#4	1	−0.160	0.209	**0.0327**
	2	−0.174	0.150	0.0303
	3	−0.229	0.159	0.0265
	4	−0.123	0.134	0.0202
#21	1	−0.834	0.555	**0.0510**
	2	−0.461	0.665	0.0479
	3	−0.590	0.577	0.0417
	4	−0.517	0.415	0.0336

Note: The higher values of RMS acceleration are in bold.
Abbreviation: RMS, root mean square.

carried out with the two boundary conditions led to the identification of the frequencies shown in Figure 12 in comparison with those experimentally identified as previously explained. The clear outcome from the comparison is that the clamped boundary condition fits with much higher precision the test results. This, whilst being in contrast with the traditional assumption of perfectly hinged behavior for both simply supported and dowel connected elements, is typical of small-amplitude vibration. In the case herein considered, indeed, even the low friction exhibiting between the floor end and its neoprene cushion support is effective in hampering rotation.

The modal shapes associated to the first 4 modes of the ground floor and roof decks are shown in Figures 13 and 14, respectively.

Concerning the ground floor deck, the first mode is translational along *Z*-axis with in-phase floor elements; the second mode is torsional along *Y*-axis with in-phase floor elements; the third mode is translational along *X*-axis with out-of-phase floor elements, where the edge floor elements tend to deform in the opposite direction of the two central ones; the fourth mode is torsional along *Y*-axis with out-of-phase floor elements.

Concerning the roof deck, where the absence of the central transverse repartition beams lowers the mutual collaboration of the floor elements, the first mode is translational along *Z*-axis with in-phase floor elements; the second mode is globally torsional along *Y*-axis with in-phase floor elements, but being the deformed shape of the single floor elements mainly translational along *Z*-axis; the third mode is translational along *X*-axis with out-of-phase floor elements where the edge floor elements tend to deform in the opposite direction of the two central ones; the fourth mode is again translational along *X*-axis with out-of-phase floor elements where adjacent floor elements tend to deform in the opposite direction; the fifth mode in torsional along *Y*-axis with out-of-phase floor elements.

With the aim to compare the numerical modal shapes with the experimental ones, the following method has been employed: (a) the results from two heel-drop tests have been analyzed per each floor—one test with longitudinal instrument disposition and one test with transverse instrument disposition; (b) the resulting acceleration time histories of each accelerometer have been filtered with a bandpass (0.5 Hz) filter in the proximity of the frequency values associated to each mode, thus isolating the vibrational component of each single mode; (c) the initial transitory part of the signal has been cut keeping the free-vibration part only; (d) the accelerations in the positions of the test accelerometers and in the instant of a vibration peak have been plotted (black dots in Figures 15 and 16). Since the equation of motion of displacement and acceleration of an SDOF system under impulsive load have the same trend scaled by a factor *C* and out-of-phase by an angle Φ, the relative accelerations plotted in Figures 15 and 16 are representative of the modal shapes of the ground floor and roof decks, respectively

$$v(t) = \frac{I}{m\omega_D} e^{-\xi\omega t} \mathrm{sen}(\omega_D t), \tag{2}$$

$$\frac{\ddot{v}(t)}{C} = \frac{I}{m\omega_D} e^{-\xi\omega t} \sin(\omega_D t + \phi). \tag{3}$$

The numerical modal shapes, extracted from the numerical models through cut views along the two lines of

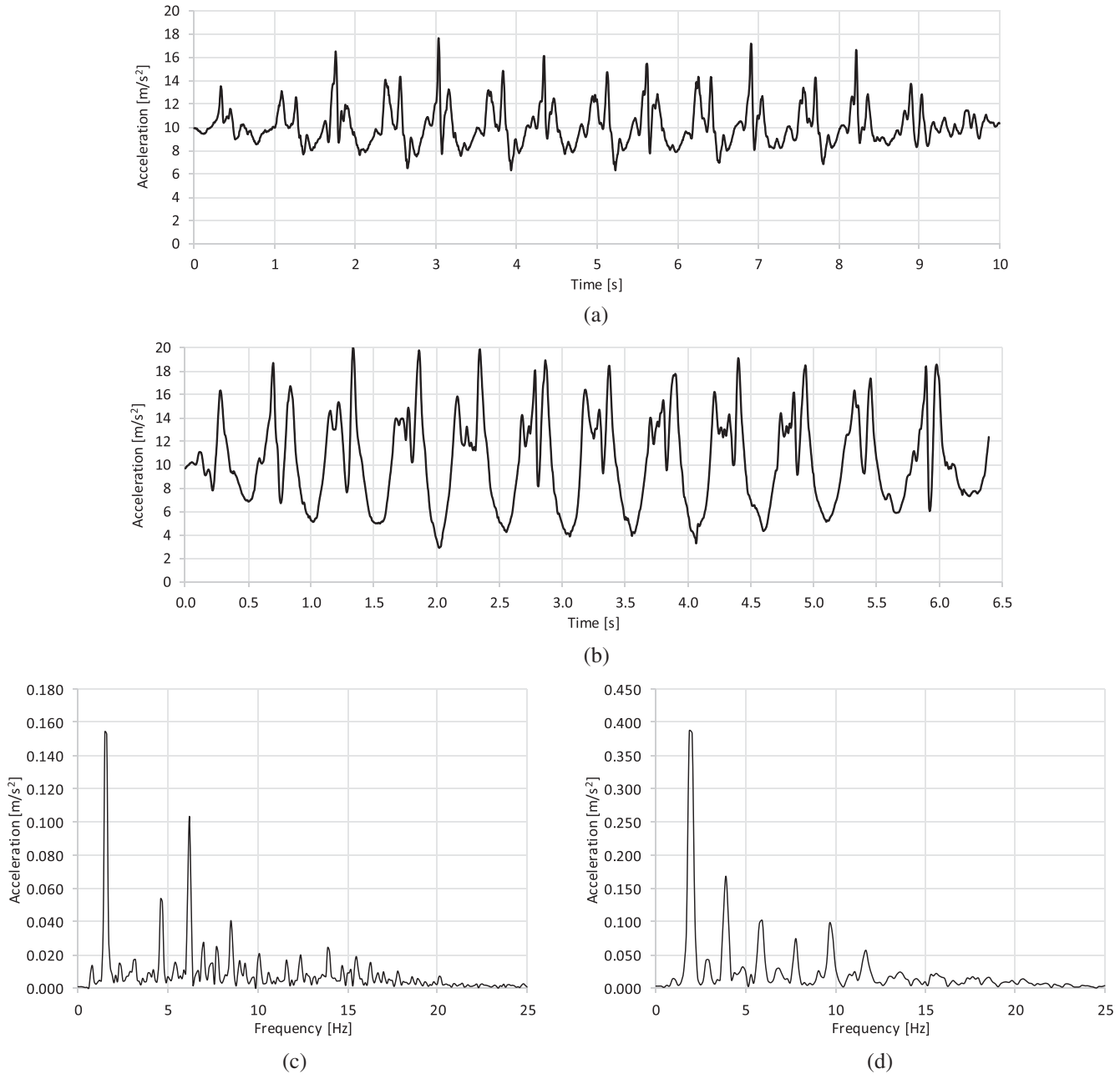

FIGURE 11 Smartphone recording of input signal: (a) time history—Pedestrian A (Test #3); (b) time history—Pedestrian B (Test #4); (c) FFT—Pedestrian A (Test #3); (d) FFT—Pedestrian B (Test #4)

installation of the accelerometers indicated in Figure 4, are superimposed to the experimental ones in Figures 15 and 16.

The Modal Assurance Criterion (MAC), proposed by Allemang and Brown[54] is used to compare the similarity of the mode shapes coming from the numerical (NUM) model and the ones identified from the experimental campaign (EXP). If the mode shapes are identical, the MAC value will be one (a mode shape compared to itself leads to a MAC value indeed one). If the mode shapes are very different, the MAC value will be close to zero. An EXP mode is well reproduced whenever the NUM mode shares the same modal period and the two have a high value of MAC. From the analysis of the ground floor deck, a positive correlation can be inferred as the MAC values are sufficiently high (above 0.8 for all the modes), with a value that increases with the mode number (Figure 17). Preliminary analysis of the experimental and numerical data allowed to reliably carry out the MAC procedure for the ground floor, since the experimental

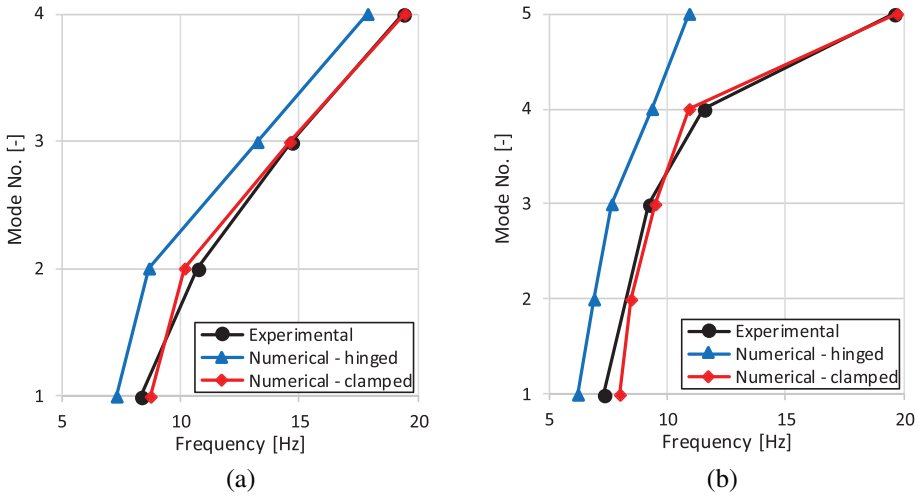

FIGURE 12 Experimental/numerical comparison of results of frequency analysis: (a) ground floor deck; (b) roof deck

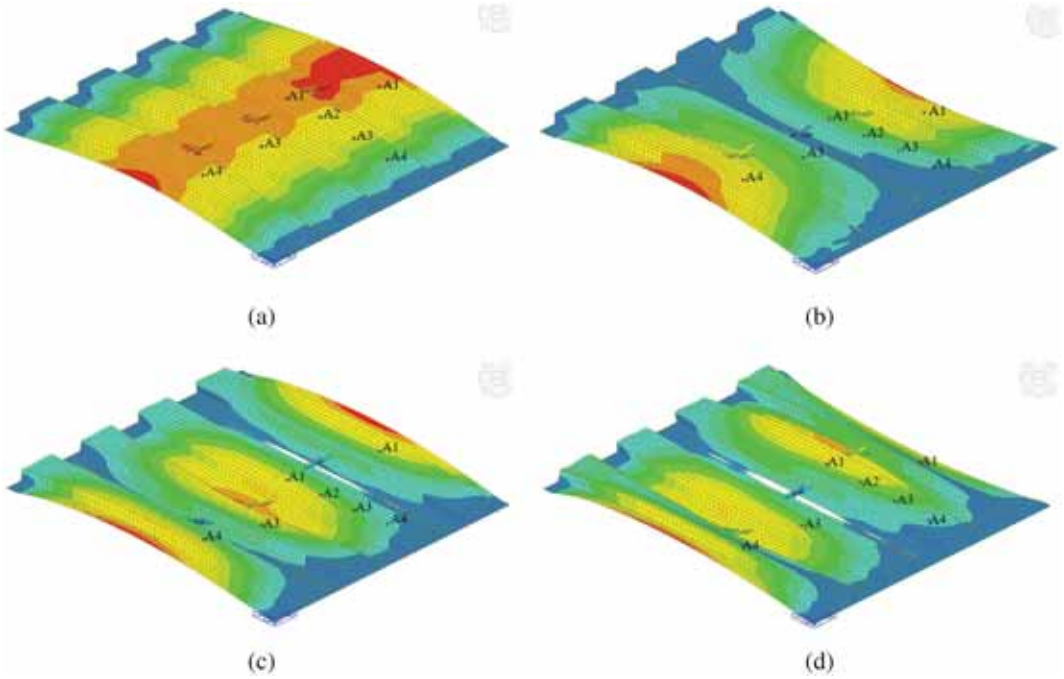

FIGURE 13 Numerical modal shapes for ground floor deck: (a) Mode 1; (b) Mode 2; (c) Mode 3; (d) Mode 4. Color contours indicate absolute displacement

measure points appeared to be sufficient to clearly identify and separate the modal shapes of different modes. However, the same analysis showed that this is not possible for the available data referring to the roof deck, due to the presence of only two measurement points in the deck transverse direction.

Nevertheless, the qualitative comparison of the two decks (Figures 15 and 16), and the quantitative comparison of the ground floor deck (Figure 17) confirm a good matching of experimental and numerical modal shapes, validating the modeling strategy employed to identify the dynamic properties of the decks.

6 | NUMERICAL SIMULATION: TIME HISTORY ANALYSIS

A further step of the research consisted in simulating the dynamic time history behavior of the decks under the different human loading test conditions. For the sake of brevity, only the main results referred to the ground floor slab are presented.

Concerning the heel-drop impulsive tests, the action has been modeled as shown in Figure 18 following the recommendations of ISO 10137:2007. The point load applied in the centroid of the pedestrian during the test

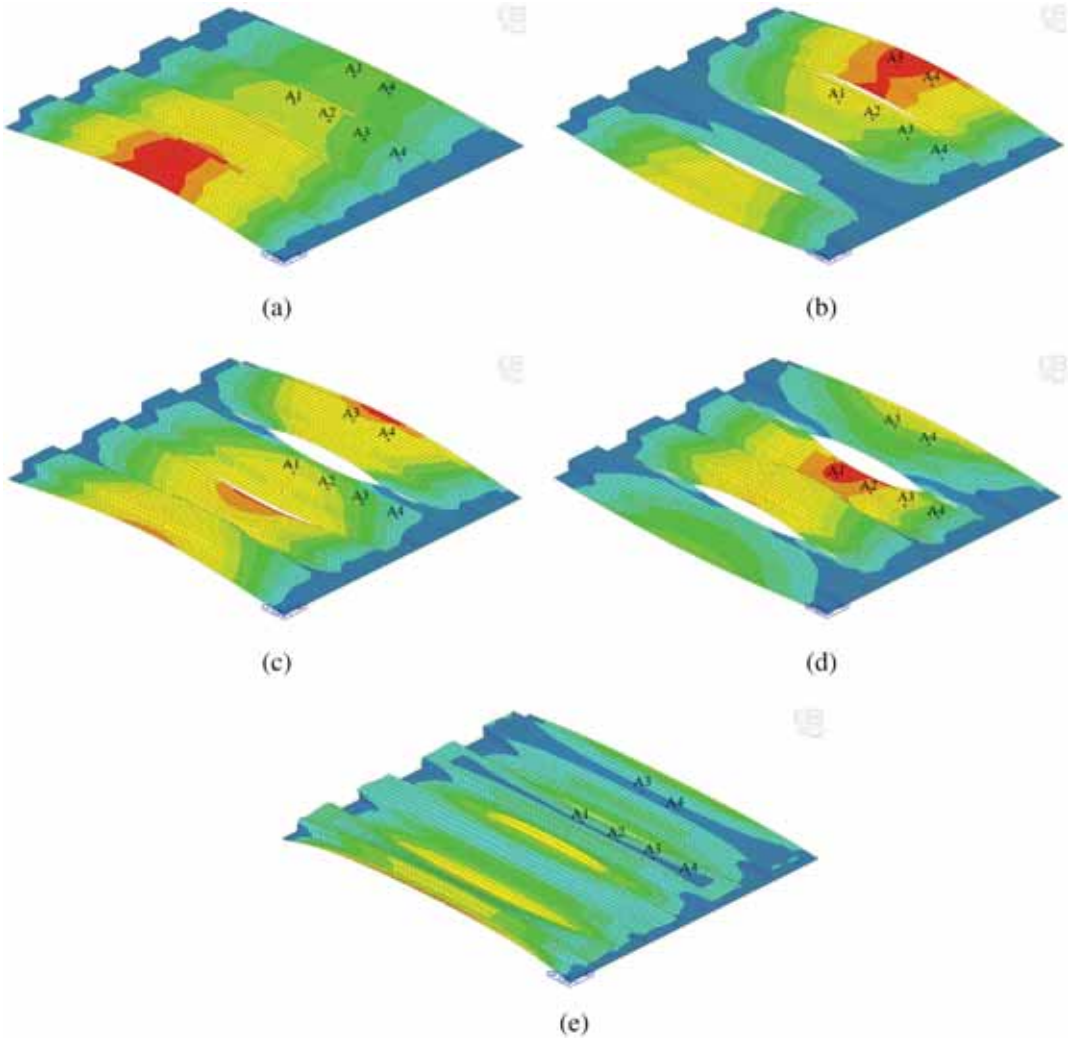

FIGURE 14 Numerical modal shapes for roof deck: (a) Mode 1; (b) Mode 2; (c) Mode 3; (d) Mode 4; (e) Mode 5. Color contours indicate absolute displacement trends

starts with the value of the pedestrian weight; a maximum impulsive load of four times the weight of the pedestrian has been introduced due to a drop height of about 20 cm; the total duration of the impulsive load is 0.05 s. A constant modal viscous damping of 1% has been attributed to all modes, following the experimental observations.

The numerical acceleration time histories corresponding to the test conditions #1 and #10 are shown in Figure 19. The comparison with the test results shown in Figure 9 shows a good matching of both maximum acceleration values and vibration history, as provided in Table 5, thus corroborating the validity of the modeling strategy. This comment is also supported by the comparison of numerical and experimental RMS acceleration values computed with the same time window T, which are in reasonable agreement.

Concerning the walking tests, three modeling strategies of the load action have been considered: (I) discontinuous; (II) continuous periodical; (III) continuous by test recording. It is observed that all the mentioned strategies, aimed at catching the experimentally measured floor behavior, have a deterministic nature, although a common load modeling approach for the evaluation of the problem concerns the application of a probabilistic analysis by means of modal superposition of the modal forces obtained by weighting of the physical forces by the mode-shape amplitudes of the walking paths for all modes of vibration contributing to the response.[55–58]

I. The discontinuous action is obtained following Baumann and Bachmann,[59] where several concentrated forces are applied to the deck (Figure 20a) in correspondence of each step. The forces are properly applied shifted in time so to represent the walking forces of the pedestrian. The single step load, shown in Figure 20a for both pedestrians, which accounts for the alternate contact of the toe and the heel, is

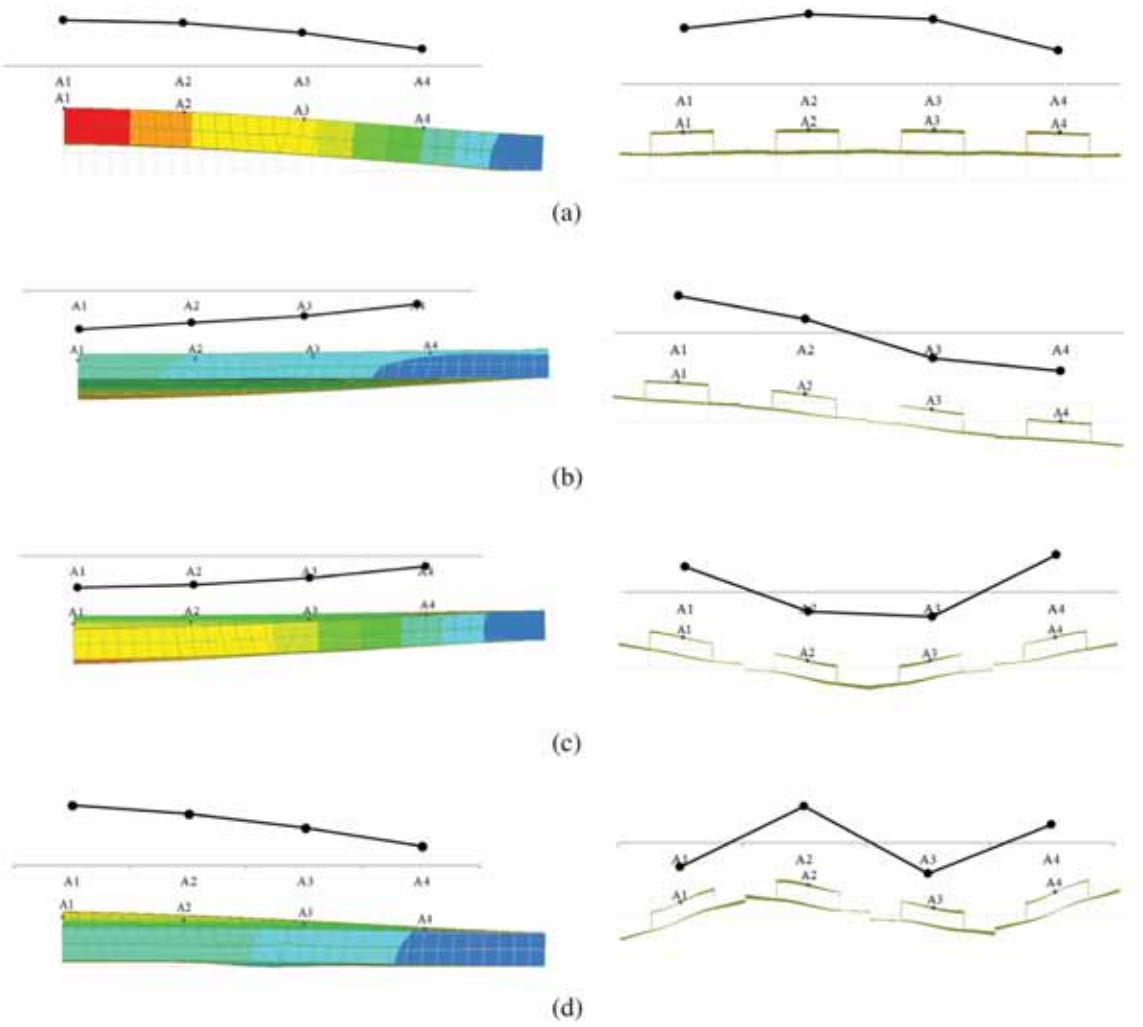

FIGURE 15 Experimental/numerical comparison of modal shapes for ground floor deck through longitudinal and transverse sections: (a) Mode 1; (b) Mode 2; (c) Mode 3; (d) Mode 4

applied with the mean experimental step frequency f_p and length of a stride of 1.625 Hz—0.84 m and 2.03 Hz—0.91 m for Pedestrians A and B, respectively.

II. The continuous periodical action is obtained following Bachmann and Amman,[22] where a single concentrated force is applied at midspan of the deck (Figure 20b). The action $F_p(t)$ is expressed as the sum of n sinusoids, where n is the number of harmonics considered (Equation 4). As suggested in the above-cited paper, the first 3 harmonics are deemed as sufficient to model the vertical component of the acceleration induced by a pedestrian, and thus Equation (4) leads directly to Equation (5), where ΔG_1, ΔG_2, and ΔG_3 are set equal to $0.4G$, $0.1G$, and $0.1G$, respectively (with G the weight of the pedestrian); Φ_1, Φ_2, and Φ_3 are set equal to 0°, 90°, and 90°, again following the above-cited paper:

$$F_p(t) = G + \sum_{i=1}^{n} G\alpha_i \times \sin\left(2\pi f_p t - \phi_i\right), \tag{4}$$

$$F_p(t) = G + \Delta G_1 \sin\left(2\pi f_p t - \Phi_1\right) + \Delta G_2 \sin\left(4\pi f_p t - \Phi_2\right) + \Delta G_3 \sin\left(6\pi f_p t - \Phi_3\right). \tag{5}$$

The curves shown in Figure 20b are those corresponding to each pedestrian.

I. The continuous recording approach was set up with the original untreated signals acquired by the smartphone installed over each pedestrian. The vertical component of these accelerations, multiplied by G, give the input action applied as a point force at midspan of the deck (Figure 20c).

The vertical component acceleration time histories are collected in Figures 21 and 22 for each walking by

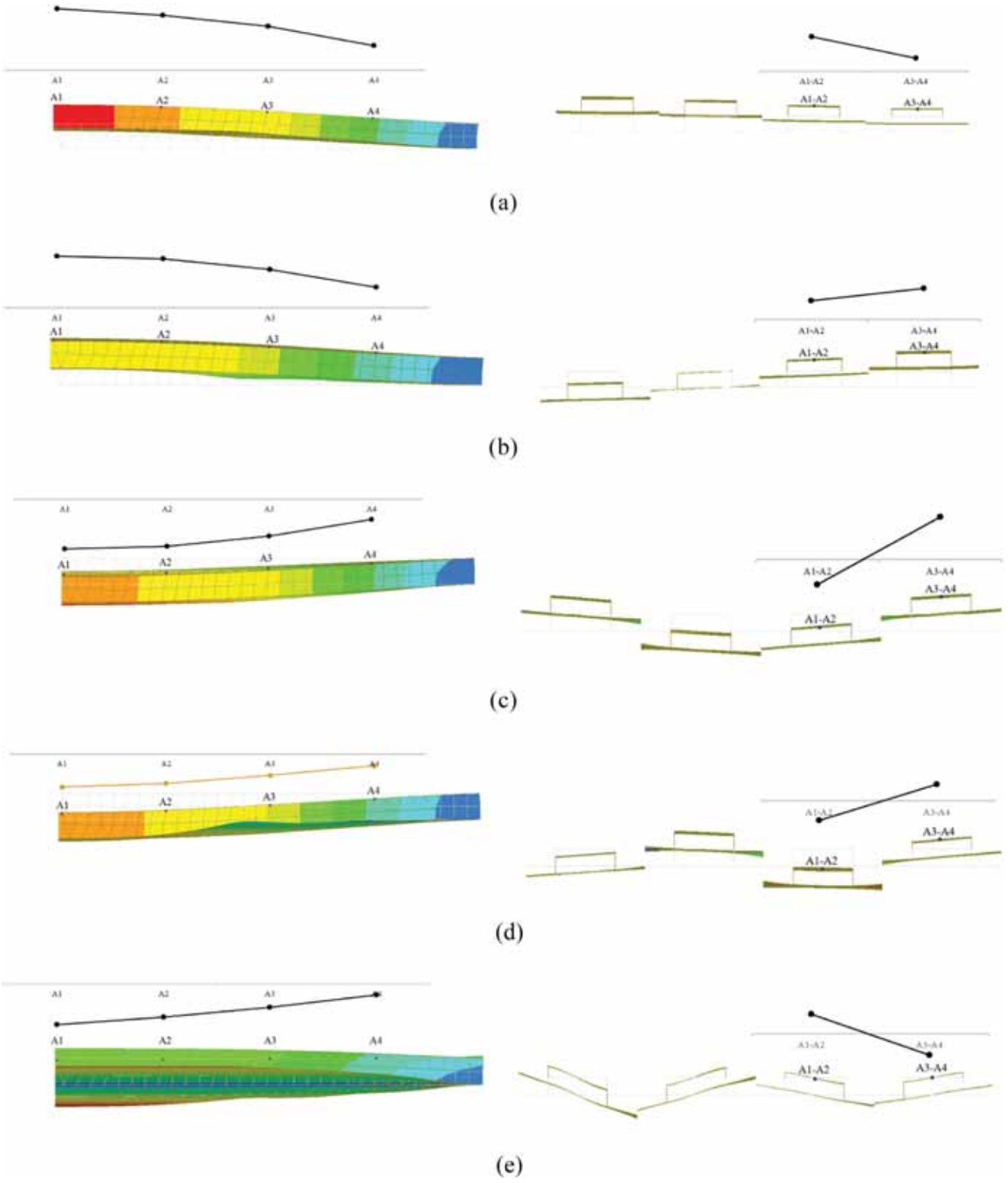

FIGURE 16 Experimental/numerical comparison of modal shapes for roof deck through longitudinal and transverse sections: (a) Mode 1; (b) Mode 2; (c) Mode 3; (d) Mode 4; (e) Mode 5

Pedestrians A and B, respectively. It is immediately perceivable that the curves are very different both in terms of maximum acceleration values and of behavior over time, with the curves associated to Strategies (I) and (II) exhibiting a much smaller response with respect to that associated to Strategy (III).

In terms of development of vibration, the curves associated to Strategy (I) are the only one in which the progressive approaching (and distancing) of the pedestrian with respect to an accelerometer can be caught. As a matter of fact, Strategies (II) and (III), relying on a single position of load application, cannot catch this phenomenon. This is the reason why a direct comparison of the curves from Strategies (II) and (III) with the experimental results of Tests #3 and #4 shown in Figure 10 cannot be done. However, the results from a comparison in terms of RMS acceleration are collected in Table 6 with reference to the instrument at midspan only, since it is the point where the loading history was applied in the numerical model. As previously noted, with Strategies (II) and (III), the load is fixed over the structure, and does not approach the position of each instrument, as in the walking tests, and therefore a comparison of the RMS accelerations recorded in other positions besides the midspan would be questionable.

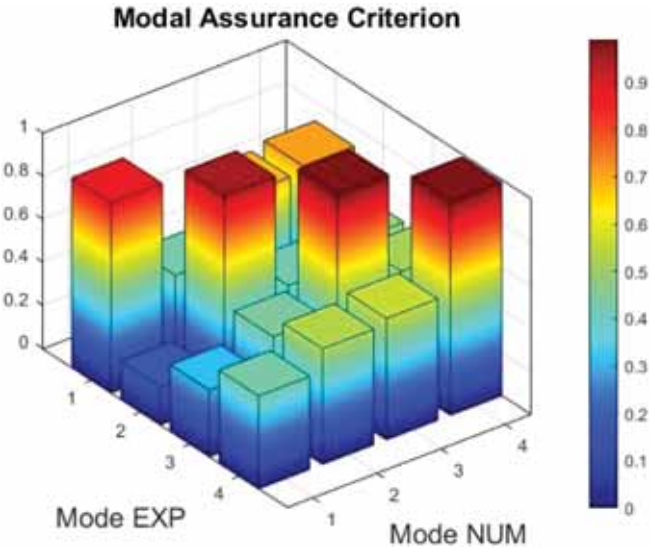

FIGURE 17 MAC procedure evaluating the degree of matching of experimental (EXP) and numerical (NUM) modal shapes

The comparison shows that both Strategies (I) and (II) provide RMS acceleration values which are about one order of magnitude lower of the experimental one, thus leading to a rough simulation of the phenomenon and on the unsafe side. Contrarily, the results of Strategy (III) provide comparable values of RMS acceleration with respect to the experimental ones, thus electing this strategy as the most accurate and reliable to catch the vibrational phenomenon for the structure herein considered.

The reason behind this clear discrepancy among the results from different strategies is to be attributed to the richness of frequency content of the smartphone-recorded signal (Strategy III), compared to the low-frequency content of the input signal of Strategies (I) and (II). In particular, the so-called high-frequency decks with fundamental frequency higher than 8 Hz can be excited to resonance in their first mode by the higher harmonics of the step frequency. In the case of Strategy (II), the highest harmonic considered (the 3rd) was equal to 4.88 and 6.09 Hz for Pedestrians A and B, respectively, which are clearly far from exciting the first natural frequency of the deck under investigation.

In order to check the above statement, a further time history analysis following Strategy (II) has been carried out by defining the load action in terms of the first 4 harmonics of the step, as per (6), where ΔG_1, ΔG_2, ΔG_3, and ΔG_4 are set equal to $(0.6\mathrm{f_p} - 0.41)G$, $0.2G$, $0.1G$, and $0.05G$, respectively; Φ_1, Φ_2, Φ_3, and Φ_4 are set equal to 0°, −90°, 180°, and 90°, again following.[22]

$$\mathrm{F_p}(t) = G + \Delta G_1 \sin\left(2\pi \mathrm{f_p} t - \Phi_1\right) + \Delta G_2 \sin\left(4\pi \mathrm{f_p} t - \Phi_2\right) + \Delta G_3 \sin\left(6\pi \mathrm{f_p} t - \Phi_3\right) + \Delta G_4 \sin\left(8\pi \mathrm{f_p} t - \Phi_4\right). \quad (6)$$

The resulting input curve is shown in Figure 23a for Pedestrian B with the experimental step frequency $\mathrm{f_p}$ set at 2.03 Hz. The response resulting from the time history analysis reported in Figure 23b shows again a response

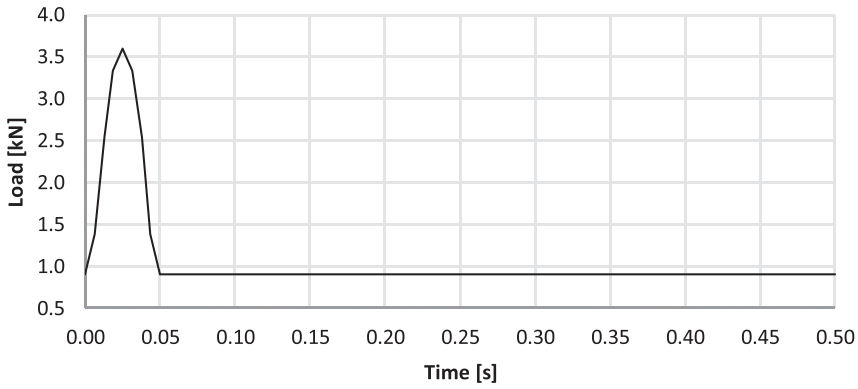

FIGURE 18 Load time history employed for heel-drop impact tests

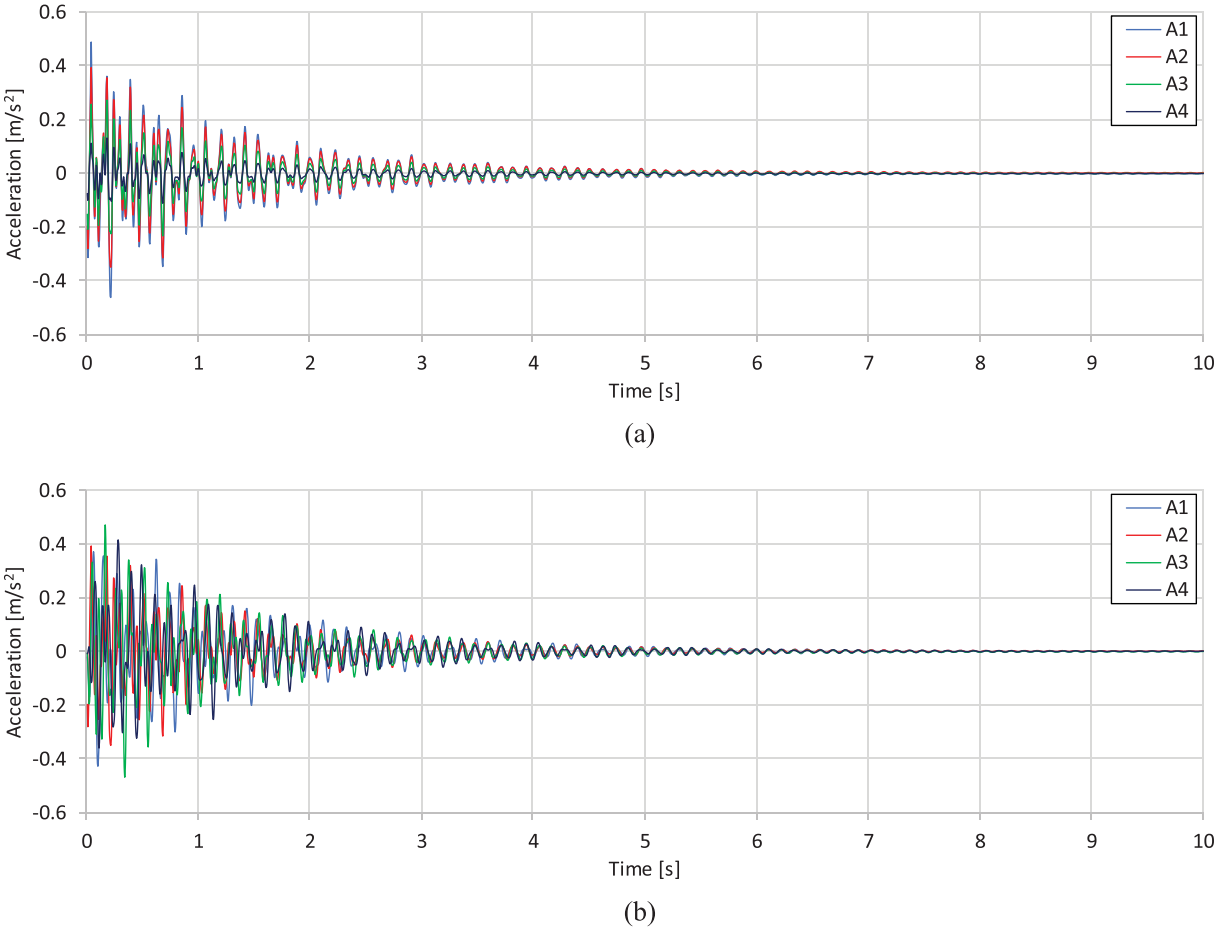

FIGURE 19 Acceleration time histories from numerical simulations of heel-drop impact tests: (a) Test #1; (b) Test #10

TABLE 5 Results of numerical simulations of heel-drop impact tests

Test ID	Accelerometer	NUM. Peak negative (m/s^2)	NUM. Peak positive (m/s^2)	NUM. RMS (m/s^2)	NUM. RMS/EXP. RMS (−)
#1	1	−0.461	0.489	**0.0625**	0.969
	2	−0.350	0.390	0.0532	0.906
	3	−0.233	0.273	0.0378	0.848
	4	−0.110	0.132	0.0174	0.724
#10	1	−0.338	0.445	0.0541	0.955
	2	−0.494	0.400	**0.0619**	1.163
	3	−0.407	0.447	0.0587	1.066
	4	−0.301	0.338	0.0455	0.941

Note: The higher values of RMS acceleration are in bold.
Abbreviations: EXP., experimental; NUM., numerical; RMS, root mean square.

much smaller than the experimental one. A further analysis carried out by imposing on purpose resonance between the fourth harmonic of the step frequency and the fundamental frequency of the deck ($f_p = 8.74/4 = 2.19$ Hz) showed a completely different response (Figure 23c), with values that finally become closer to the real one due to the imposed resonance, as shown in Table 7.

This confirms that input signals poor in frequency content can hardly predict a resonant-like dynamic interaction between human walking and deck

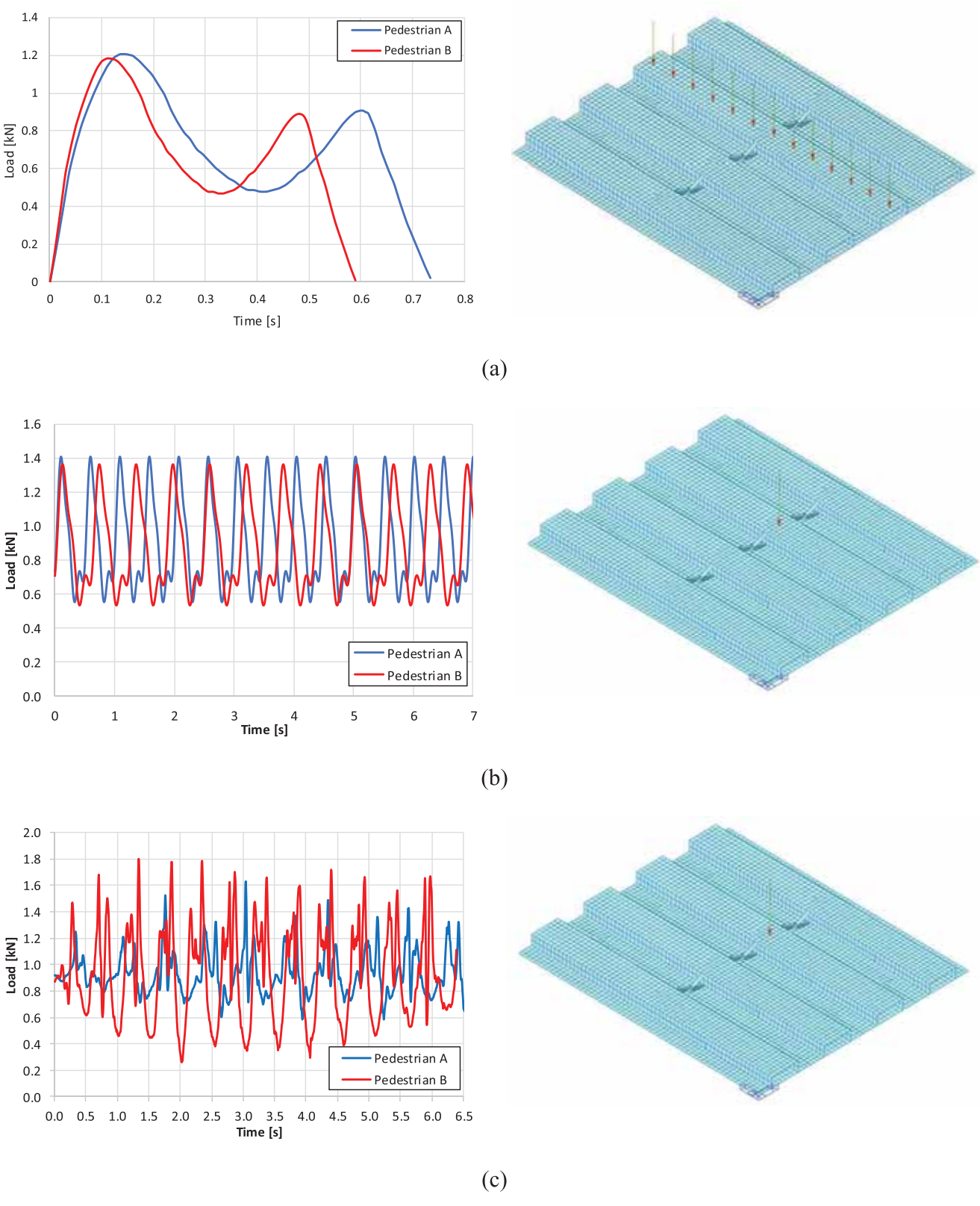

FIGURE 20 Modeling strategy of the loading function: (a) I—discontinuous; (b) II—periodic continuous; (c) III—smartphone-recorded time history

vibration, unless (a) the number of harmonics considered is enough to excite the deck close to its natural frequencies, and (b) a wide range of frequency steps is considered so to catch that exact one which takes the deck to resonance. Furthermore, this observation provides another confirmation of the importance of

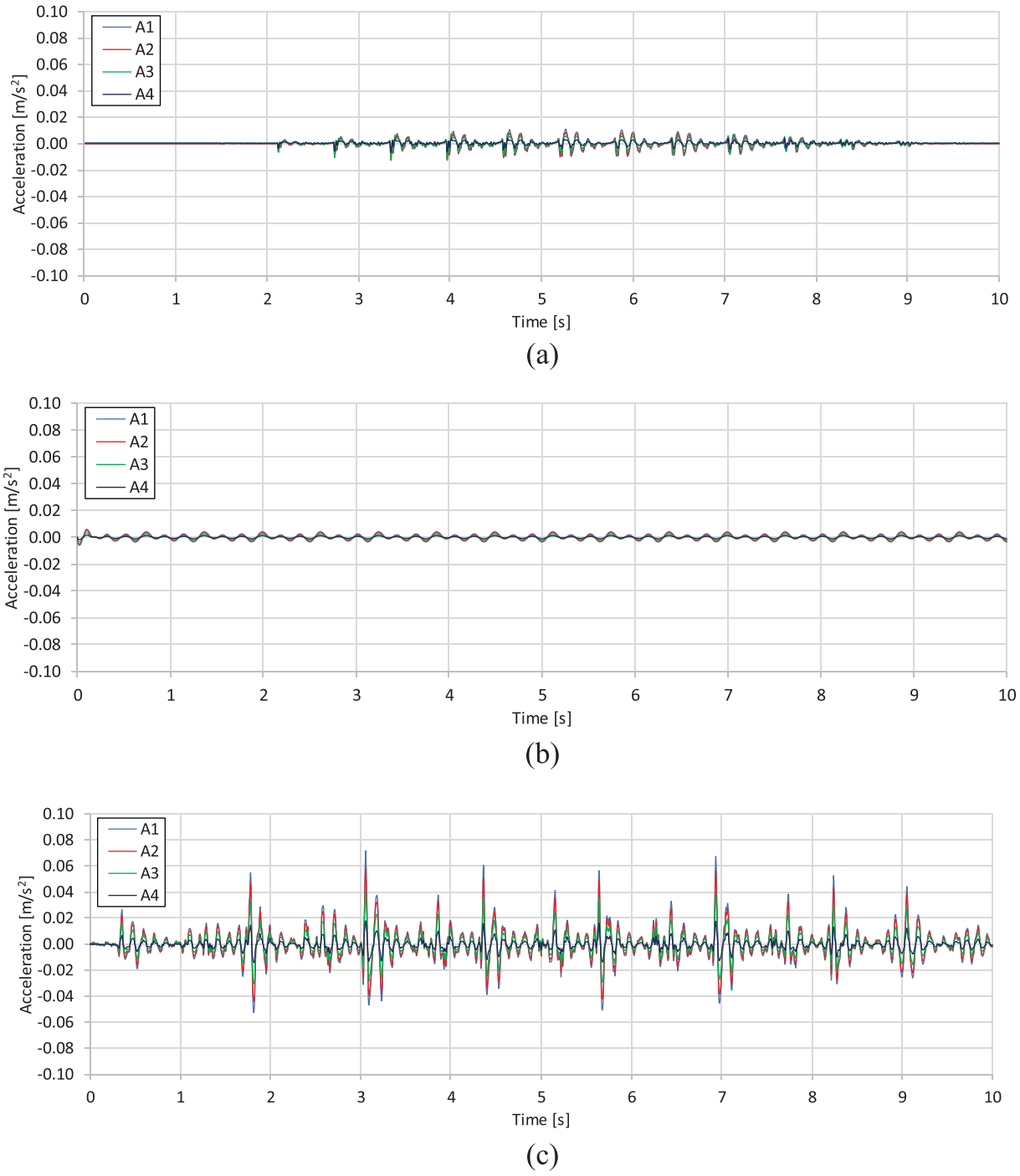

FIGURE 21 Acceleration time histories from numerical simulations of Walking Test #3 with modeling strategy: (a) I—discontinuous; (b) II—periodic continuous; (c) III—smartphone-recorded time history

recording the walking signal and to use it in the analyses for vibration check.

7 | PARAMETRIC INVESTIGATION

After the deck modeling details and the load action strategy have been validated, a parametric investigation has been carried out to investigate the role of transverse restraint conditions, geometry of the floor elements, mass and equivalent viscous damping (EVD) on the issue of the perception of vibrations for the deck technology under investigation. Several decks configurations have been analyzed by changing the parameters as shown in Table 8. The baseline condition consisted in a deck unit larger than the previously described one subjected to testing: the baseline deck is made by five-floor elements with

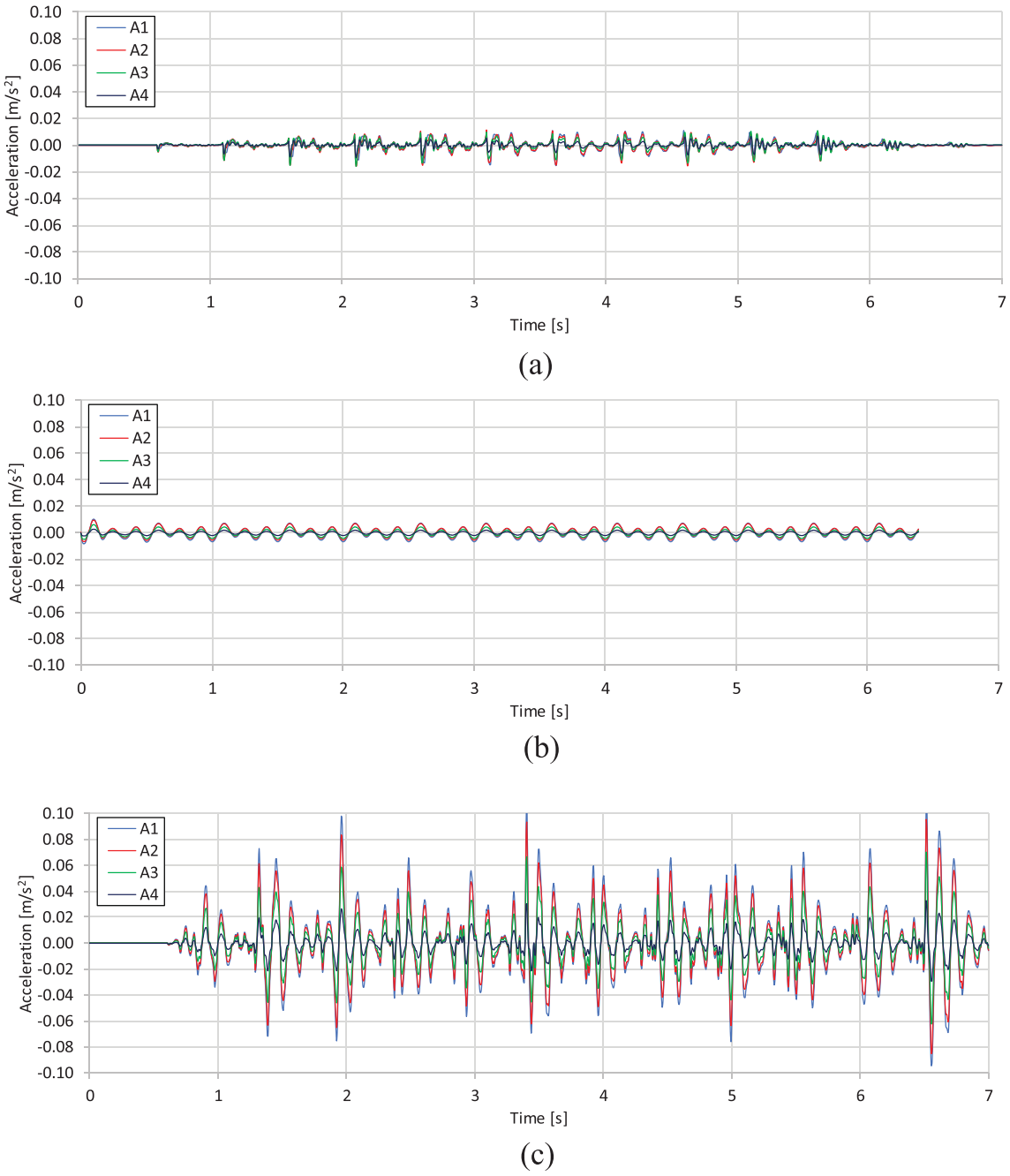

FIGURE 22 Acceleration time histories from numerical simulations of Walking Test #4 with modeling strategy: (a) I—discontinuous; (b) II—periodic continuous; (c) III—smartphone-recorded time history

TABLE 6 Results of numerical simulations of walking tests with different modeling strategies

Test ID	Modeling strategy	Max RMS (m/s^2)	Max RMS NUM./EXP. (–)
#3	I	0.00278	0.205
#4	I	0.00342	0.105
#3	II	0.00214	0.158
#4	II	0.00399	0.122
#3	III	0.01310	0.963
#4	III	0.02769	0.846

Abbreviations: EXP., experimental; NUM., numerical; RMS, root mean square.

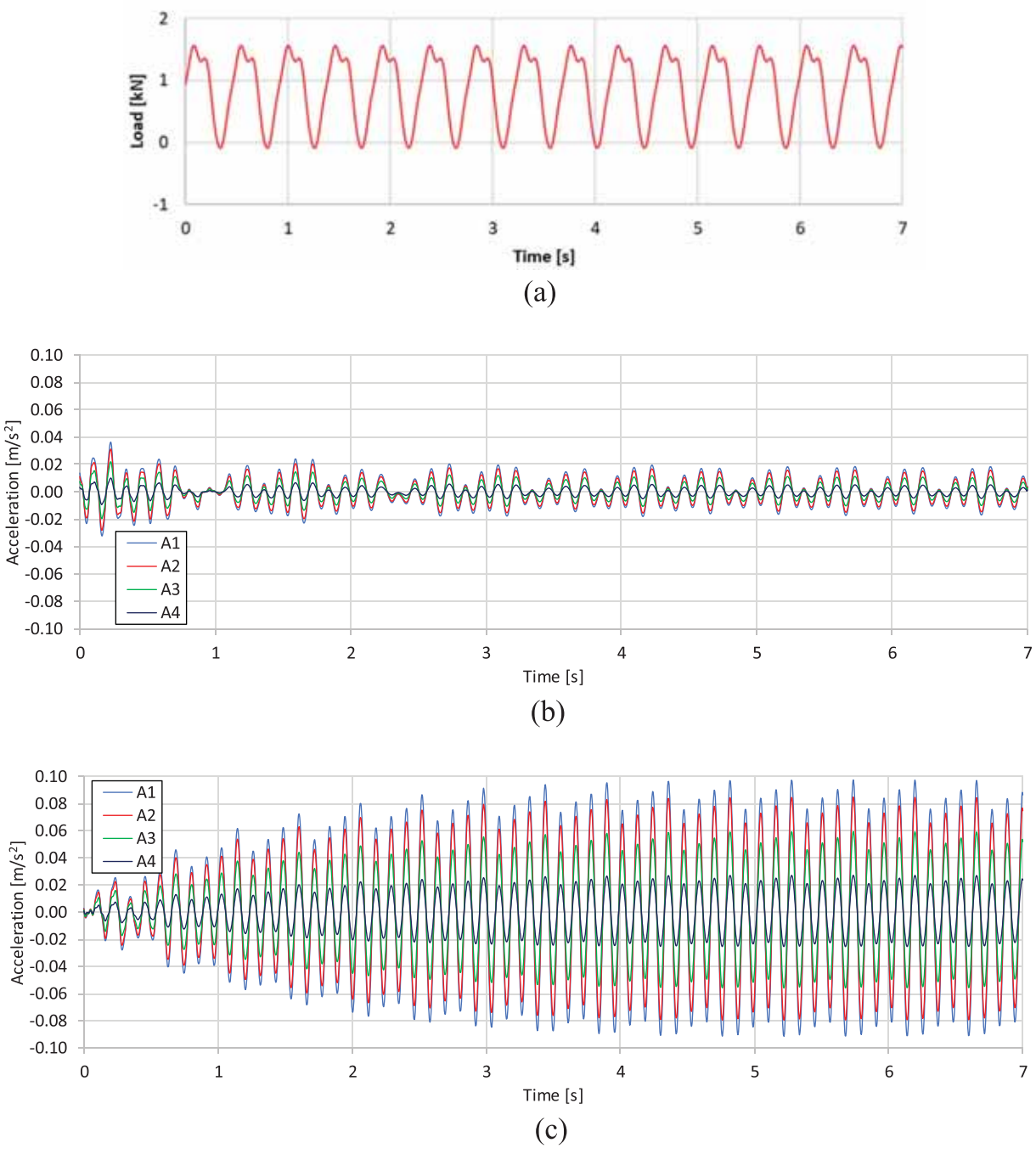

FIGURE 23 Updated analysis with 4-harmonics periodic continuous modeling (Strategy II): (a) walking modeling of Pedestrian B; (b) acceleration time history with experimental step frequency; (c) acceleration time history with adapted step frequency for imposed resonance

TABLE 7 Results of numerical simulations of walking tests

TEST ID	Modeling strategy	Step frequency (Hz)	Max RMS (m/s^2)	Max RMS NUM./EXP. (–)
#4	II (4 harmonics)	2.072	0.00423	0.075
#4	II (4 harmonics)	2.185	0.05635	0.995

Note: Updated analysis with 4-harmonics periodic continuous modeling.
Abbreviations: EXP., experimental; NUM., numerical; RMS, root mean square.

TABLE 8 Decks considered in the parametric analysis

Deck condition	Mutual welding scheme	Central transverse beam	Connection to cladding beam	Length (m)	Depth (m)	Spread mass (kg/m^2)	EVD (%)
Baseline	6-Edge	Crosses	No	12	0.35	650	3
§01	**No**	**No**	No	12	0.35	650	3
§02	6-Edge	**No**	No	12	0.35	650	3
§03	**3-Centre**	**No**	No	12	0.35	650	3
§04	**3-Centre**	Crosses	No	12	0.35	650	3
§05	**3-Centre**	**Top struts**	No	12	0.35	650	3
§06	6-Edge	Crosses	**Yes**	12	0.35	650	3
§07	6-Edge	Crosses	No	**11**	0.35	650	3
§08	6-Edge	Crosses	No	**10**	0.35	650	3
§09	6-Edge	Crosses	No	12	**0.40**	650	3
§10	6-Edge	Crosses	No	12	0.35	**750**	3
§11	6-Edge	Crosses	No	12	0.35	**550**	3
§12	6-Edge	Crosses	No	12	0.35	650	**1**
§13	6-Edge	Crosses	No	12	0.35	650	**2**
§14	6-Edge	Crosses	No	12	0.35	650	**4**
§15	6-Edge	Crosses	No	12	0.35	650	**5**

Note: Variations from baseline deck are in bold.
Abbreviation: EVD, equivalent viscous damping.

the same cross-section as in Figure 1a, but assumed to be 12 m long, placed adjacently and mutually connected by a central transverse repartition beam made with X-shaped steel angle crosses and with six welds per edge in the positions indicated in Figure 24a. This baseline condition represents the most severe structural condition of the investigated deck technology, which also yields to the higher propensity for vibration issues. The other models in Figure 24 show all the different solutions for the transverse restraints investigated.

A single time history analysis has been performed on each deck condition. The loading strategy previously defined as Strategy III was employed, where the recorded signal of Pedestrian B has been used. After the analyses, the acceleration histories of different positions along the deck have been extracted, from which the corresponding spectrum in one-third octave band in the frequency interval 1–80 Hz was derived in Decibel. Afterward, the spectrum has been filtered with a ponderation filter determined on the basis of human perception of vibrations. The pondered frequency acceleration has been finally reconverted into RMS acceleration and compared with the requirements from ISO 10137 for residential/office environments.

A further check considering the simplified design approach outlined in the HIVOSS document has also been carried out with the same deck conditions. In this case, the fundamental frequency and the associated participating mass have been evaluated from a modal analysis of the numerical model, and have been used to calculate the OS-RMS90 value defined in HIVOSS. Then, the performance class of the decks has been assessed basing on the tables available in the HIVOSS guidelines and compared with the suggested requirements for residential/office environments.

The results are collected in Table 9. The RMS acceleration for the baseline case is far beyond the limit suggested in ISO 10137 by 1.52. This suggests that this particular condition of the deck, which has been checked against ULSs and SLS for deflection, would not perform satisfactorily from a vibrational point of view unless remedial actions are taken. As such, the SLS for vibration is predominant for its proper design.

By analyzing the results of the other deck conditions, it is evident that different transverse restraint conditions including absence or other shaping of transverse repartition beam and absence of other positioning of edge welds, only slightly affect the problem. The only efficient solution found is the one where the transverse repartition beam is welded to the edge concrete beams, belonging to the cladding panel elements. Being these beams stiff in bending, they modify the behavior of the deck from predominantly unidirectional to bidirectional, introducing a

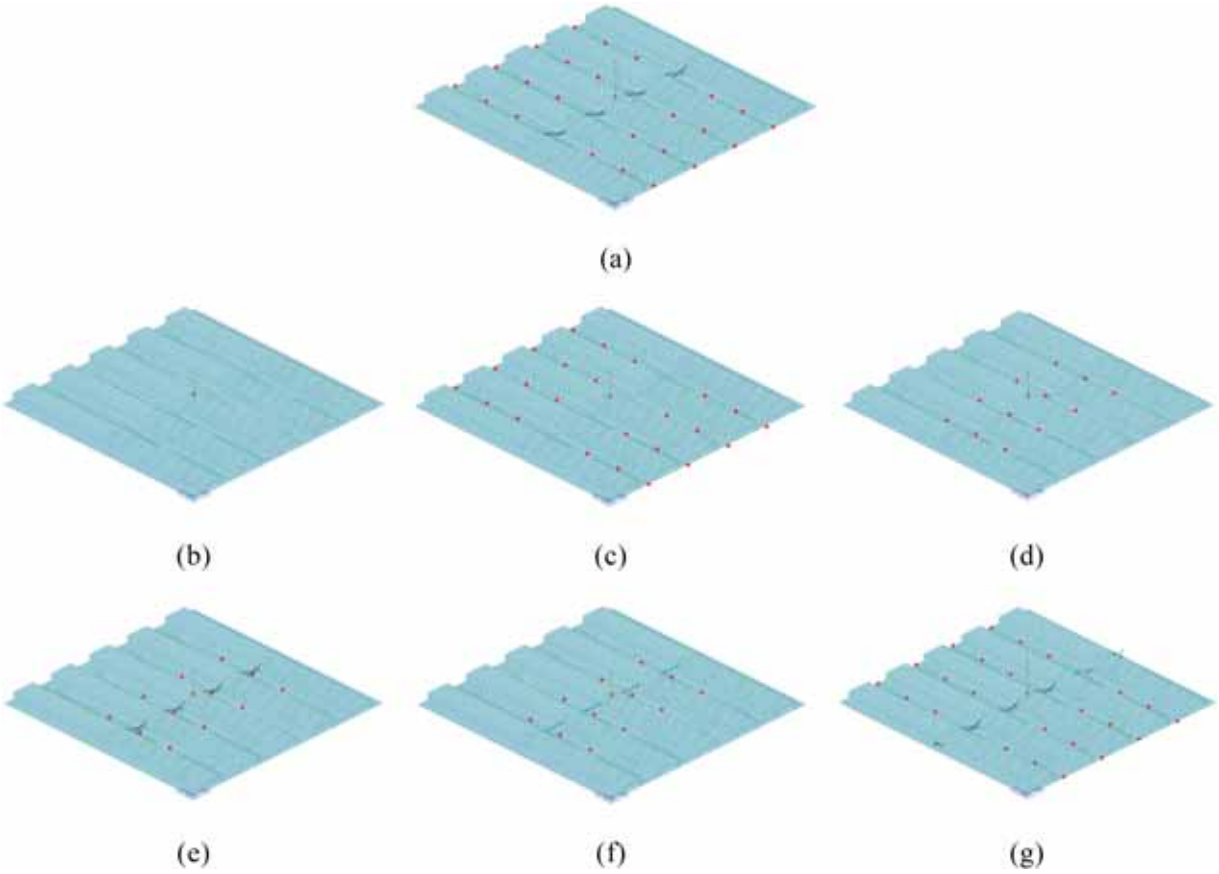

FIGURE 24 Different transverse restraint conditions of the deck: (a) baseline deck with six flange edge welds and crosses transverse beam; (b) fully independent floor elements; (c) six flange edge welds; (d) three flange central welds; (e) three flange central welds and crosses transverse beams; (f) three flange central welds and struts transverse beams; (g) six flange welds and crosses transverse beams also connected with the edge cladding beam

tendency to behave more like a peripherally supported solid plate. This is also confirmed by the increase of the fundamental frequency, associated with the vertical translation mode. This solution, however, brings large force values to the cladding panel element, through the transverse beam elements. This element, then, should be carefully checked and probably over-proportioned with respect to the deck conditions previously considered.

Contrarily, the geometric conditions of the deck play an important role on the RMS acceleration check, being the reduction of span from 12 to 11 or 10 m enough to reduce the ratio of the resulting RMS acceleration over the RMS limit suggested by ISO 10137 down to 0.96 or 0.93, respectively, thus complying in both cases. Even more influence is played by the slab stiffness, in fact increasing its depth to 0.4 m, keeping the same flanges, brings to a dramatic reduction of the RMS acceleration value, which, as a consequence, results largely satisfied even with a span of 12 m.

Modifications of the mass plays in a tricky way on the RMS acceleration value, since both a 15% increase or decrease of mass brings to a reduction of the RMS value, although not below the limits set forth in ISO 10137. In particular, the 15% increase of mass leads to a reduction of the frequencies of the deck, thus separating the natural frequency associated to the 3rd structural mode from the 5th step harmonic (see Figure 11d), although the 1st mode is again close the third harmonic. A 15% decrease of mass, despite decreasing the transient time to resonance, separates both the first and the third modes from the closer harmonics, providing a better vibrational response.

Finally, the effect of the variation of the modal EVD over the value of RMS acceleration is strong, as expected due to the low initial values, but not resolutive. Increasing the modal damping from 1% to 2% with respect to the critical one corresponds to a reduction of the RMS acceleration ratios from 3.56 to 2.15, which is still much larger than the baseline situation (1.39). An increase of the damping to 4% or 5%, however, leads to a further reduction of the RMS acceleration, but not sufficient to pass the check. Even higher values of EVD would be required, which can be, in principle, achieved by adding vibration control devices such as tuned mass dampers, whose cost,

TABLE 9 Results of the parametric analysis

Condition	f_1 (Hz)	f_2 (Hz)	f_3 (Hz)	f_4 (Hz)	RMS (mm/s^2)	RMS/$RMS_{baseline}$ (−)	$RMS/RMS_{limit,ISO10137}$ (−)	OS-RMS_{90} (m/s^2)	HIVOSS class (−)
Baseline	6.04	6.60	9.70	13.47	30.408	1.00	**1.52**	1.8	D
§01	6.04	6.33	8.09	10.51	27.870	0.92	**1.39**	1.8	D
§02	6.04	6.44	8.77	11.69	26.959	0.89	**1.35**	1.8	D
§03	6.04	6.44	9.00	12.13	28.893	0.95	**1.44**	1.8	D
§04	6.04	6.56	9.85	13.69	31.423	1.03	**1.57**	1.8	D
§05	6.04	6.45	9.03	12.19	29.571	0.97	**1.48**	1.8	D
§06	6.99	9.53	12.91	16.48	18.122	0.60	0.91	1.6	D
§07	7.18	7.68	10.77	14.58	19.270	0.63	0.96	1.4	D
§08	8.40	8.84	11.90	15.73	18.651	0.61	0.93	0.8	D
§09	7.00	7.59	11.02	14.96	16.172	0.53	0.81	1.2	D
§10	5.73	6.29	9.24	12.83	23.342	0.77	**1.17**	2.2	D
§11	6.43	6.98	10.25	14.23	20.563	0.68	**1.03**	1.6	D
§12	6.04	6.60	9.70	13.47	71.190	2.34	**3.56**	4.0	**E**
§13	6.04	6.60	9.70	13.47	43.089	1.42	**2.15**	2.4	D
§14	6.04	6.60	9.70	13.47	24.733	0.81	**1.24**	1.6	D
§15	6.04	6.60	9.70	13.47	20.452	0.67	**1.02**	1.2	D

Note: Negative checks are in bold.
Abbreviations: OS-RMS, one step-root mean square; RMS, root mean square.

and required volume, are however important parameters to determine their applicability.

A different scenario appears when referring to the checks in the HIVOSS guidelines, with only the deck arrangement §12 (EVD = 1%) leading to a performance class "critical." This points out the higher permissibility of this approach deriving from being based on a statistical approach.

8 | CONCLUSIONS

The analysis of a structural prototype employing a novel precast construction system for 26 human-induced vibration tests carried out on the ground and roof slabs allowed to characterize the vibrational behavior of the floor slabs as intermediate between resonant and impulsive with fundamental frequencies of the first mode around 8 Hz. The equivalent viscous damping associated to the first modes was estimated to be close to 1%; this relatively low value is mostly due to the absence in the prototype of finishes, furnishing and internal partitions.

The comparison of numerical results from frequency analysis and experimental outcomes clearly showed that the proper end conditions for the floor elements, despite being simply supported on elastomeric pads or connected with dowels to the bearing wall panels, are full clamps, due to the small vibration amplitude of the slabs induced by human walking.

The adopted modeling strategy was first checked against the experimental results in terms of both frequencies and mode shapes, and later employed to simulate the dynamic tests. The standard strategy for the definition of the impact load from heel-drop, calibrated with the properties of the pedestrians, provided a sound time history simulation of the vibration. For the simulation of walking loads activity, three strategies for the application of the loading were investigated: (I) discontinuous, with as many concentrated forces as the pedestrian steps following the Baumann-Bachmann approach; (II) continuous, applied at the midspan, based on the summation of harmonics following the Bachmann–Amman approach; (III) continuous, applied at the midspan, with application of a load derived from the acceleration signal recorded by smartphones positioned nearby the walking person center of gravity. Both Strategies (I) and (II) (where in Strategy (II), three harmonics were considered, following standard recommendations) were inefficient in catching the vibration history and its amplitude, underestimating the latter by about one order of magnitude. Strategy (III), instead, provided much better results,

highlighting the benefits of the smartphone recording (whose reliability was previously checked against recording from professional accelerometers) of the input loading history. The main reason for this outcome is related to the frequency content of the artificial load action for both Strategies (I) and (II), whereas the signal used in Strategy (III) is natural and contains a richer spectrum of frequencies. Strategy (II) provides a reliable response only when the load step frequency is almost an exact submultiple of the fundamental frequency of the deck; this might require the use of more than three harmonics.

The results from parametric dynamic time-history analyses on models employing the experimentally validated strategy highlighted that different mutual floor-to-floor connections, including transverse repartition beams, have only a marginal influence, apart from the case when the transverse repartition beam is welded to the edge cladding beams, which modifies the unidirectional deck behavior into a bidirectional one; the span of floor elements and especially their stiffness have great influence; reasonable variations of mass and damping variations have moderate influence. The investigated conditions were also checked with both ISO and HIVOSS procedures, resulting mostly negative with the first deterministic approach and mostly positive with the latter probabilistic approach. Being the issue of annoyance induced by perception of vibrations very subjective, the authors are not able to state whether the ISO approach is too severe or the HIVOSS too permissive for the investigated cases (also considering the deterministic modeling approach adopted), although the use of ISO appears more conservative and on the safe side. The vibrational behavior in service of the precast deck technology under investigation turns out to be a key issue for a correct structural design, which could become critical. The outcome from the simplified experimental program, interpretation of the results, numerical modeling strategies, and parametric analysis allowed to frame the issue and is deemed to provide a useful tool for similar cases to be investigated in the future.

ACKNOWLEDGMENTS

The authors would like to thank Marcello Catena for his contribution in carrying out the analyses. They also thank Angelo Basso from the precast concrete manufacturer Antonio Basso Spa of Treviso, Italy, for the assistance during testing at their premises and Marco Cucchi from the laboratory LPMSC of Politecnico di Milano for the assistance on the use of the test instrumentation.

DATA AVAILABILITY STATEMENT

The data that support the findings of this study are available upon direct request to the authors.

ORCID

Bruno Dal Lago https://orcid.org/0000-0002-3088-8376
Luca Martinelli https://orcid.org/0000-0002-0491-3363
Francesco Foti https://orcid.org/0000-0002-0339-4653

REFERENCES

1. Dal Lago B. Experimental and numerical assessment of the service behaviour of an innovative long-span precast roof element. Int J Conc Struct Mat. 2017;11(2):261–73.
2. Dal Lago B, Bisi D, Ferrara L. On the application of basalt-fibre reinforced polymer (BFRP) bars to prestressed slab elements typical of the precast concrete industry. ACI SP-333: Advances in Concrete Bridges: Design, Construction, Evaluation, and Rehabilitation. 2019;333:40–59.
3. CEN-EN 1990: 2002. Eurocode - basis of structural design. Brussels, Belgium: European Committee for Standardization.
4. CEN-EN 1992: 2005. Eurocode 2 – design of Concrete Structures. Brussels, Belgium: European Committee for Standardization.
5. Allen DE, Rainer JH. Vibration criteria for long span floors. Can J Civ Eng. 1976;3(2):165–73.
6. Allen DE, Rainer JH, Pernica G. Vibration criteria for long span concrete floors. ACI SP-60: Vibrations in Concrete Structures. 1979;60:67–78.
7. Allen DE, Murray TM. Design criterion for vibrations due to walking. AISC Eng J. 1993;30:117–29.
8. Matsumoto Y, Sato S, Nishioka T, Shiojiri H. A study on design of pedestrian over-bridges. Trans JSCE. 1972;9:63–70.
9. Wheeler J. Prediction and control of pedestrian induced vibration in footbridges. ASCE J Struct Div. 1982;108:2045–65.
10. Zivanovic S, Pavic A, Reynolds P. Vibration serviceability of footbridges under human-induced excitation: a literature review. J Sound Vibr. 2005;279(1–2):1–74.
11. Shahabpoor E, Pavic A, Racic V. Interaction between walking humans and structures in vertical direction: a literature review. Shock Vib. 2016;2016:3430285.
12. Pavic A, Reynolds P. Modal testing and dynamic FE model correlation and updating of a prototype high-strength concrete floor. Cem Conc Comp. 2003;25:787–99.
13. Pavic A, Reynolds P, Waldron P. Modal testing and FE model correlation and updating of a long-span prestressed concrete floor. Proc Inst Civ Eng: Struct Build. 2002;152(2):97–109.
14. Pavic A, Reynolds P, Waldron P, Bennett KJ. Critical review of guidelines for checking vibration serviceability of post-tensioned concrete floors. Cem Conc Comp. 2001;23(1):21–31.
15. Zhou X, Liu J, Cao L, Li J. Vibration serviceability of prestressed concrete floor system under human activity. Struct Infrastruct Eng. 2017;13(8):967–77.
16. Cao L, Liu J, Li J, Zhang R. Experimental and analytical studies on the vibration serviceability of long-span prestressed concrete floor. Earthq Eng & Eng Vib. 2018;17:417–28.
17. Cao L, Qi H, Li J. Experimental and numerical studies on the vibration serviceability of fanshaped prestressed concrete floor. Int J Distrib Sensor Networks. 2018;14(8):1–11.
18. Liu F, Battini JM, Pacoste C, Granberg A. Experimental and numerical dynamic analyses of hollow core concrete floors. Structure. 2017;12:286–97.
19. Liu F, Battini JM, Pacoste C. Assessment of hollow-Core concrete floors against human-induced vibration. Struct Eng Int. 2020;31(3):376–90.

20. Galbraith F, Barton M. Ground loading from footsteps. J Acoust Soc Am. 1970;48(5B):1288–92.
21. Andriacchi T, Ogle J, Galante J. Walking speed as a basis for normal and abnormal gait measurements. J Biomech. 1977; 10(4):261–8.
22. Bachmann H, Ammann WJ. Vibration in structures induced by man and machines. Zurich, Switzerland: IABSE, Zürich; 1987.
23. Bachmann, H., Ammann WJ, Deischl F, Eisenmann J, Floegl I, Hirsch GH, et al.: Vibration problems in structures: practical guidelines. 1995.
24. Reiher H, Meister FJ. The effect of vibration on people. Forschung auf dem Gebeite des Ingenieurwesens. 1931;2: 381–6.
25. Wiss JF, Parmelee RA. Human perception of transient vibration. ASCE J Struct Div. 1974;100(4):773–87.
26. Han SW, Lee MJ, Moon KH, Sang W, Han SW. Acceleration thresholds of vertical floor vibrations according to human perception levels in Korea. Adv Struct Eng. 2009;12(4): 595–607.
27. ISO 10137: 2007. Bases for design of structures - serviceability of buildings and walkways against vibrations.
28. UNI 9614: 1990. Misura delle vibrazioni negli edifici e criteri di valutazione del disturbo.
29. HIVOSS - Human Induced Vibration of Steel Structures (2007) Vibration Design of Floors - Background document.
30. HIVOSS - Human Induced Vibrations of Steel Structures (2007) Vibration Design of Floors - Guideline.
31. Dal Lago B, Dal Lago A, Franceschelli F. Innovation for smart industrial housing. Conc Plant Int. 2016;2:298–300.
32. Dal Lago B, Dal Lago A. New precast constructions for integrated complex urban interventions. BFT Int. 2018;84(4): 72–80.
33. Ren R, Naito CJ. Precast concrete diaphragm connector performance database. ASCE J Struct Eng. 2013;139(1):15–27.
34. Dal Lago B, Del Galdo M, Bisi D. Tests and design of welded-bar angle connections of precast floor elements. J Adv Conc Tech. 2022;20(2):43–56.
35. Dal Lago B, Ferrara L. Efficacy of roof-to-beam mechanical connections on the diaphragm behaviour of precast decks with spaced roof elements. Eng Struct. 2018;176:681–96.
36. Dal Lago B, Bianchi S, Biondini F. Diaphragm effectiveness of precast concrete structures with cladding panels under seismic action. Bull Earthq Eng. 2019;17(1):473–95.
37. Dal Lago B, Gajera K. Progressive collapse prevention in high-rise precast buildings with box-section slab elements. Conc Plant Int. 2021;5:188–96.
38. Bournas D, Negro P, Molina FJ. Pseudodynamic tests on a full-scale 3-storey precast concrete building: behaviour of the mechanical connections and floor diaphragms. Eng Struct. 2013;57:609–27.
39. Dal Lago B, Muhaxheri M, Ferrara L. Numerical and experimental analysis of an innovative ligh
tweight precast concrete wall. Eng Struct. 2017;137:204–22.
40. Dal Lago B, Negro P, Dal Lago A. Seismic design and performance of dry-assembled precast structures with adaptable joints. Soil Dyn Earthq Eng. 2018;106:182–95.
41. Dal Lago B, Molina J. Assessment of a capacity spectrum design approach against cyclic and seismic experiments on full-scale precast RC structures. Earthq Eng Struct Dyn. 2018;47(7):1591–609.
42. Davis B, Liu D, Murray TM. Simplified experimental evaluation of floors subject to walking-induced vibration. ASCE J Perf Constr Fac. 2014;28(5):04014023.
43. Martinelli L, Racic V, Dal Lago B, Foti F. Testing walking-induced vibration of floors using smartphones recordings. Robotics. 2020;9(2):37.
44. Bitter R, Mohiuddin T, Nawrocki M. LabVIEW: advanced programming techniques. Boca Raton: CRC Press; 2006.
45. Vieyra Software. Physics Toolbox App. Version 1.9.4.6, 2020.
46. Zhao X, Han R, Ding Y, Yu Y, Guan Q, Hu W, et al. Portable and convenient cable force measurement using smartphone. J Civ Struct Health Mon. 2015;5:481–91.
47. Zhao X, Ri K, Wang N. Experimental verification for cable force estimation using handled shooting of smartphones. J Sens. 2017;6:1–13.
48. Bocian M, Brownjohn JMW, Racic V, Hester D, Quattrone A, Monnickendam R. A framework for experimental determination of localised vertical pedestrian forces on full-scale structures using wireless attitude and heading reference system. J Sound Vibr. 2016;376:217–43.
49. Shahabpoor E, Pavic A. Estimation of vertical walking ground reaction force in real-life environments using single IMU sensors. J Biomech. 2018;79:181–90.
50. Mohammed AS, Pavic A, Racic V. Improved model for human induced vibrations of high-frequency floors. Eng Struct. 2018; 168:950–66.
51. Clough RW, Penzien J. Dynamics of structures. 3rd ed. Berkeley: Computers and Structures Inc.; 2003.
52. MIDAS Information Technology. MIDAS/Gen-General structure design system. MIDAS/Gen Version 8.25 Analysis and Design Manual, Seongnam, South Korea, 2013.
53. CEN-EN 1993:2004. Eurocode 3 – design of steel structures. Brussels, Belgium: European Committee for Standardization.
54. Allemang, R.J., and Brown, D.L.: A correlation coefficient for modal vector analysis. Proceedings of the International Modal Analysis Conference, 1982, 110–116.
55. Brownjohn JMW, Pavic A, Omenzetter P. A spectral density approach for modelling continuous vertical forces on pedestrian structures due to walking. Can J Civ Eng. 2004;31(1): 65–77.
56. Piccardo G, Tubino F. Equivalent spectral model and maximum dynamic response for the serviceability analysis of footbridges. Eng Struct. 2012;40:445–56.
57. Bassoli E, van Nimmen K, Vincenzi L, Van den Broeck P. A spectral load model for pedestrian excitation including vertical human-structure interaction. Eng Struct. 2018;156: 537–47.
58. Muhammad Z, Reynolds P, Avci O, Hussein M. Review of pedestrian load models for vibration serviceability assessment of floor structures. Vibr. 2020;2:1–24.
59. Baumann K, Bachmann H. Durch menschen verursachte dynamische lasten und deren auswirkungen auf balkentragwerke. Zurich: Swiss Federal Institute of Technology (ETH); 1988.

AUTHOR BIOGRAPHIES

Bruno Dal Lago, Assistant Professor, Department of Theoretical and Applied Sciences, Università degli Studi dell'Insubria, via Dunant 3, 21100 Varese, Italy. Email: bruno.dallago@uninsubria.it

Luca Martinelli, Associate Professor, Department of Civil and Environmental Engineering, Politecnico di Milano, piazza Leonardo da Vinci 33, 20133 Milan, Italy.
Email: luca.martinelli@polimi.it

Francesco Foti, Assistant Professor, Department of Civil and Environmental Engineering, Politecnico di Milano, piazza Leonardo da Vinci 33, 20133 Milan, Italy.
Email: luca.martinelli@polimi.it

How to cite this article: Dal Lago B, Martinelli L, Foti F. Slender precast voided slabs under walking-induced vibration. Structural Concrete. 2022. https://doi.org/10.1002/suco.202100754